Historical review of experimental results in light scattering

Jesús Escobar-Cerezo

October-December, 2018

Brief concept introduction

Methodology I: Scattering matrix

$$\begin{pmatrix} I_{sc} \\ Q_{sc} \\ U_{sc} \\ V_{sc} \end{pmatrix} = \frac{\lambda^2}{4\pi^2 D^2} \begin{pmatrix} F_{11} & F_{12} & F_{13} & F_{14} \\ F_{21} & F_{22} & F_{23} & F_{24} \\ F_{31} & F_{32} & F_{33} & F_{34} \\ F_{41} & F_{42} & F_{43} & F_{44} \end{pmatrix} \begin{pmatrix} I_{in} \\ Q_{in} \\ U_{in} \\ V_{in} \end{pmatrix}$$

I_{in} → Intensity

Q_{in}, U_{in} → Linear polarization

V_{in} → Circular polarization

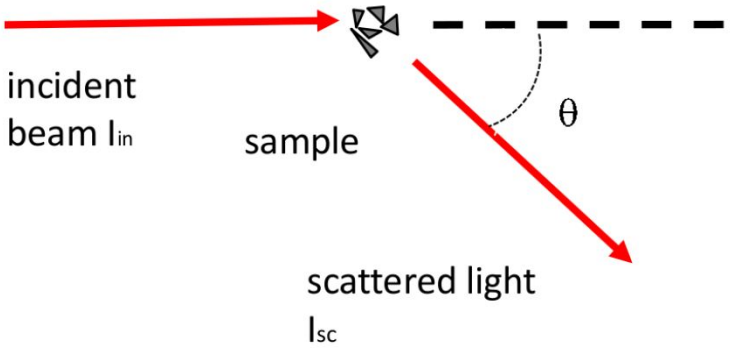

Scattering matrix depends on:

- Refractive index
- Shape
- Size distribution
- Wavelength

Size parameter

$$x = \frac{2\pi r}{\lambda}$$

Methodology I: Scattering matrix

$$\begin{pmatrix} I_{sc} \\ Q_{sc} \\ U_{sc} \\ V_{sc} \end{pmatrix} = \frac{\lambda^2}{4\pi^2 D^2} \begin{pmatrix} F_{11} & F_{12} & 0 & 0 \\ F_{12} & F_{22} & 0 & 0 \\ 0 & 0 & F_{33} & F_{34} \\ 0 & 0 & -F_{34} & F_{44} \end{pmatrix} \begin{pmatrix} I_{in} \\ Q_{in} \\ U_{in} \\ V_{in} \end{pmatrix}$$

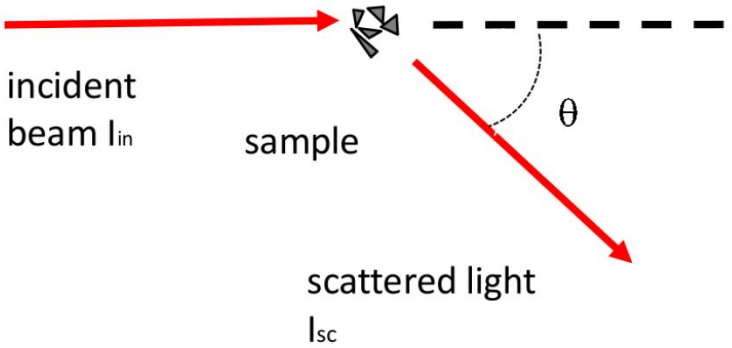

Scattering matrix depends on:

- Refractive index
- Shape
- Size distribution
- Wavelength

Size parameter

$$x = \frac{2\pi r}{\lambda}$$

Methodology I: Performance test

Degree of linear polarization for unpolarized incident light

Phase function

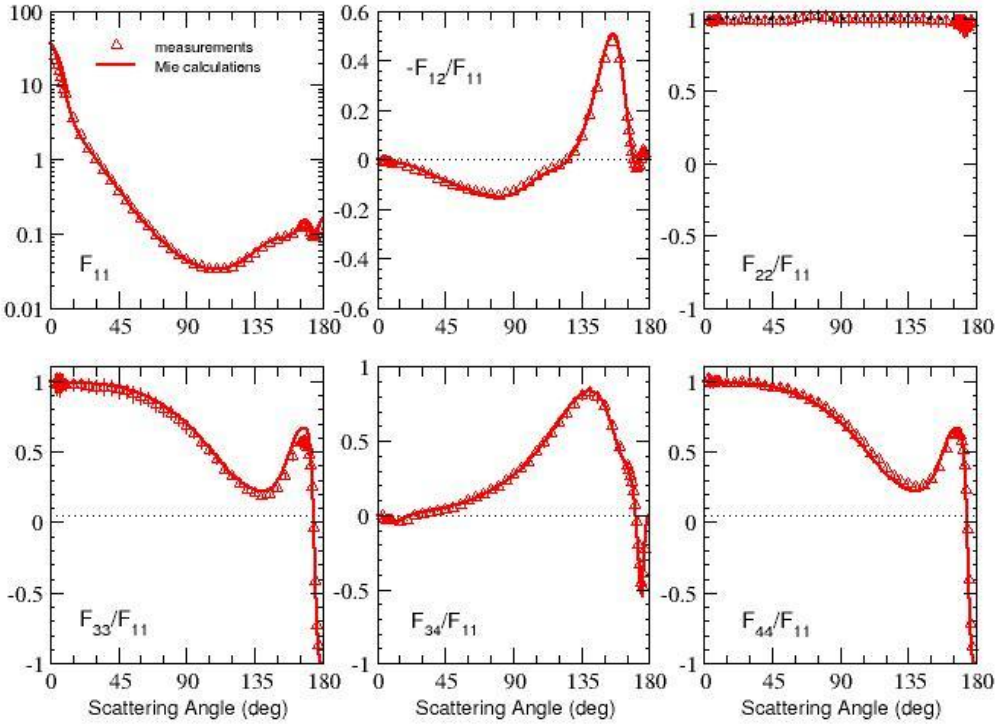

Water droplets scattering matrix

Methodology I: Performance test

Asymmetry parameter

$$g = \int_0^{\pi} \mathrm{d}\theta \sin\theta \cos\theta F_{11}^{\mathrm{syn}}(\theta)$$

Phase function

Degree of linear polarization for unpolarized incident light

Backscattering depolarization factor

$$\delta_L = \frac{F_{11}(\pi) - F_{22}(\pi)}{F_{11}(\pi) + F_{22}(\pi)}$$

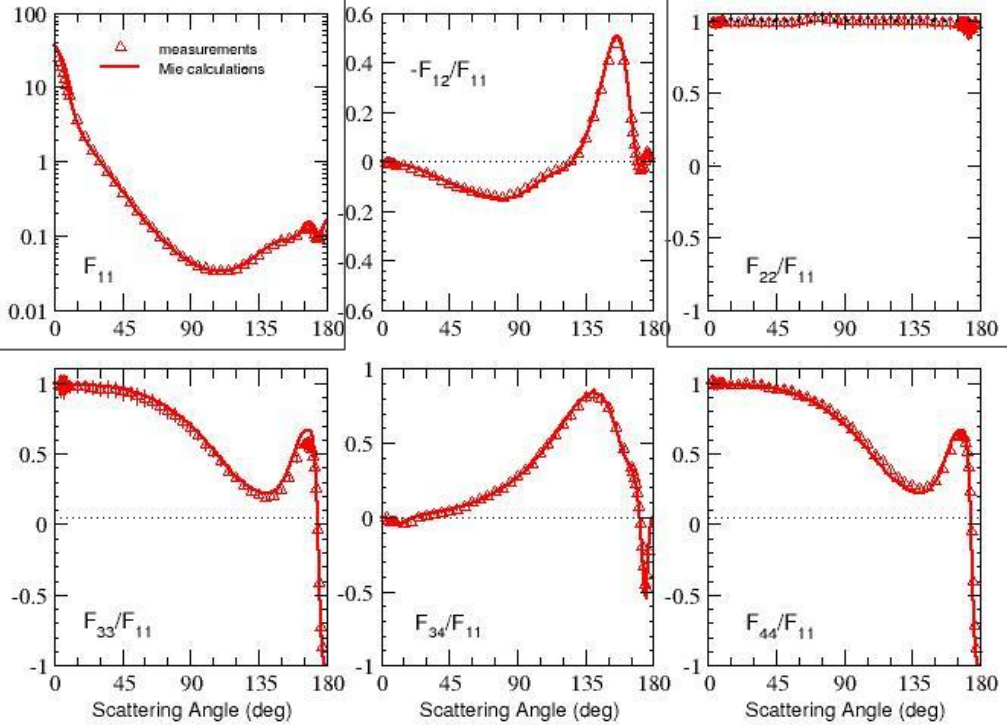

Water droplets scattering matrix

OK, now we can move on…
let’s talk about polarization

Vikings 700 A.C.

*(... not an actual image from 700 AC)

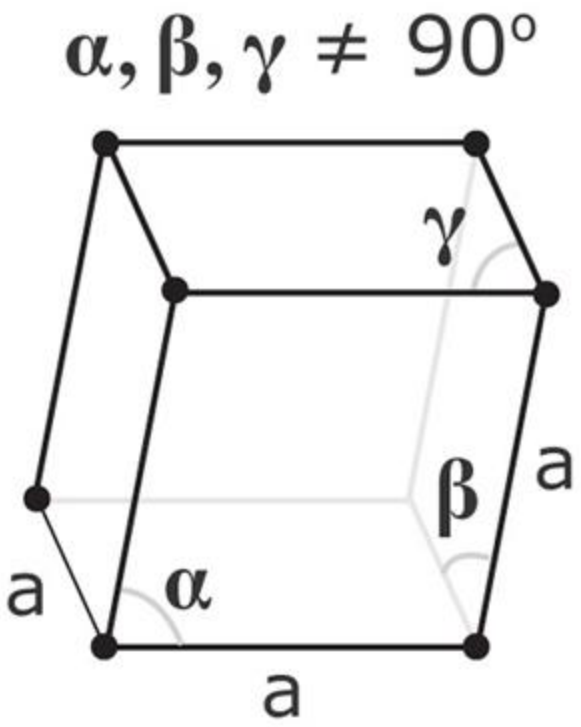

Scientific studies

Bartholin


Newton


Huygens

Rasmus Bartholin (1669): First scientific study of birefringence.

Huygens and Newton (1672)

Malus (1808)

Brewster (1812)


Malus


Brewster

Light scattering

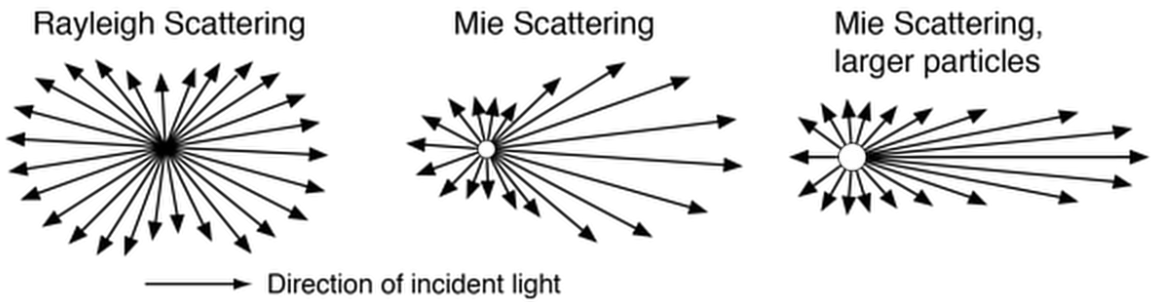

1871 1908

$$I = I_0 \left(\frac{1 + \cos^2 \theta}{2R^2} \right) \left(\frac{2\pi}{\lambda} \right)^4 \left(\frac{n^2 - 1}{n^2 + 2} \right)^2 \left(\frac{d}{2} \right)^6$$

Polarimetric studies of the Moon

Moon (NASA/Goddard/Lunar Reconnaissance Orbiter)

Polarization studies of the Moon:

1. First studies in XIX century.

2. Those studies were constrained to certain lunar phases.

3. Suggested materials: very polished surfaces of glass, igneous rock or even ice.

Polarimetric studies of the Moon

Moon (NASA/Goddard/Lunar Reconnaissance Orbiter)

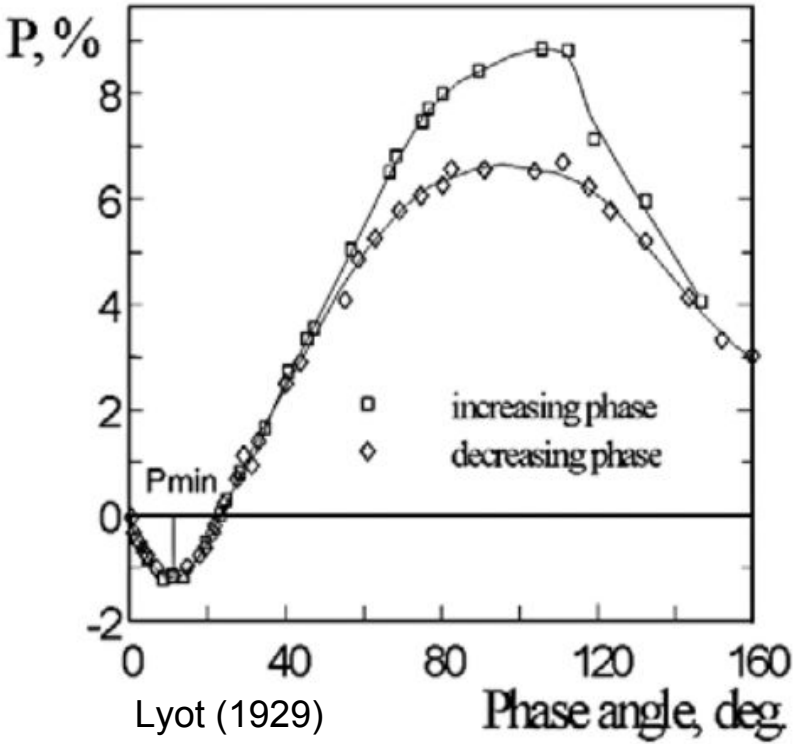

Lyot (1929)

1974 - Venus atmosphere

Interpretation of the Polarization of Venus

JAMES E. HANSEN

Goddard Institute for Space Studies, New York, N. Y. 10025

J. W. HOVENIER

Dept. of Physics and Astronomy, Free University, Amsterdam, Netherlands

(Manuscript received 20 November 1973, in revised form 15 January 1974)

1. Introduction

Venus is our nearest planetary neighbor, yet one of the most mysterious. To a large extent this is due to the veil of clouds surrounding the planet. These clouds not only mask Venus, but their own composition is unknown. Many possible compositions have been suggested in the literature, including water, H_2O ice, solid CO_2, carbon suboxide (C_3O_2; Sinton, 1953; Kuiper, 1957; Harteck *et al.*, 1963), hydrated ferrous chloride ($FeCl_2 \cdot 2H_2O$; Kuiper, 1969), NaCl (Hunten, 1968), formaldehyde (CH_2O; Wildt, 1940), hydrocarbons (Velikovsky, 1950; Hoyle, 1955; Kaplan, 1963), hydrocarbon-amide polymers (Robbins, 1964), polywater (Donahue, 1970), ammonium nitride ($NH_4 \cdot NO_2$; Dauvillier, 1956), calcium and magnesium carbonates (Öpik, 1961), NH_4Cl (Lewis, 1968; Hunten and Goody, 1969), mercury and mercury compounds (Lewis, 1969; Rasool, 1970) and aqueous solutions of hydrochloric acid ($HCl \cdot nH_2O$; Lewis, 1972; Hapke, 1972) and sulfuric acid ($H_2SO_4 \cdot nH_2O$; Sill, 1972; Young and Young, 1973; Young, 1973). Although a large amount of theoretical and observational effort has been expended on this problem, no consensus on the cloud composition has evolved.

Our best means for investigating the clouds of Venus material should be consistent with. However, these features have proved insufficient for either a specific identification of the cloud particles or eliminating most proposed compositions, in part because it is always possible to hypothesize a gaseous absorber, an admixture of another cloud material, or a lower cloud layer to provide the observed absorption. There have been concerted attempts to link several weaker features in the spectral reflectivity to specific cloud compositions, particularly H_2O ice (Sagan and Pollack, 1967) and $FeCl_2 \cdot 2H_2O$ (Kuiper, 1969); however, the features which were associated with ice (other than the absorption at $\lambda \approx 3$ μm) have also been credited to gaseous CO_2 absorption (cf. Rea and O'Leary, 1968), and a number of the features associated with ferrous chloride are of doubtful reality (cf. Cruikshank and Thomson, 1971).

A different sort of evidence on the cloud composition is provided by the angular distribution of reflected light, both the distribution of brightness over the planetary disk and the disk-integrated brightness as a function of planetary phase angle. Arking and Potter (1968) analyzed such observations for Venus by comparing them with multiple scattering computations for spherical cloud particles. They found agreement with

1974 - Venus atmosphere

Some considerations

Phase matrix

$$\mathbf{P}(\alpha)=\begin{bmatrix} P^{11} & P^{21} & 0 & 0 \\ P^{21} & P^{22} & 0 & 0 \\ 0 & 0 & P^{33} & -P^{43} \\ 0 & 0 & P^{43} & P^{33} \end{bmatrix},$$

Normalization condition

$$\frac{1}{4\pi}\int_{4\pi} P^{11}(\alpha)\,d\omega = 1,$$

$$\mathbf{P}=\frac{1}{1+f}\mathbf{P}_c+\frac{f}{1+f}\mathbf{P}_R,$$

Cloud particles

Rayleigh contribution

$$r_{\text{eff}}=\frac{\int_{r_1}^{r_2} r\pi r^2 n(r)\,dr}{\int_{r_1}^{r_2} \pi r^2 n(r)\,dr}.$$

Effective radius

$$v_{\text{eff}}=\frac{\int_{r_1}^{r_2} (r-r_{\text{eff}})^2 \pi r^2 n(r)\,dr}{r_{\text{eff}}^2 \int_{r_1}^{r_2} \pi r^2 n(r)\,dr},$$

Effective variance

Number size distribution

$$n(r)=\text{constant}\times r^{(1-3b)/b} e^{-r/ab} \qquad \left.\begin{matrix} a=r_{\text{eff}} \\ b=v_{\text{eff}} \end{matrix}\right\},$$

(Effect of changes in size)

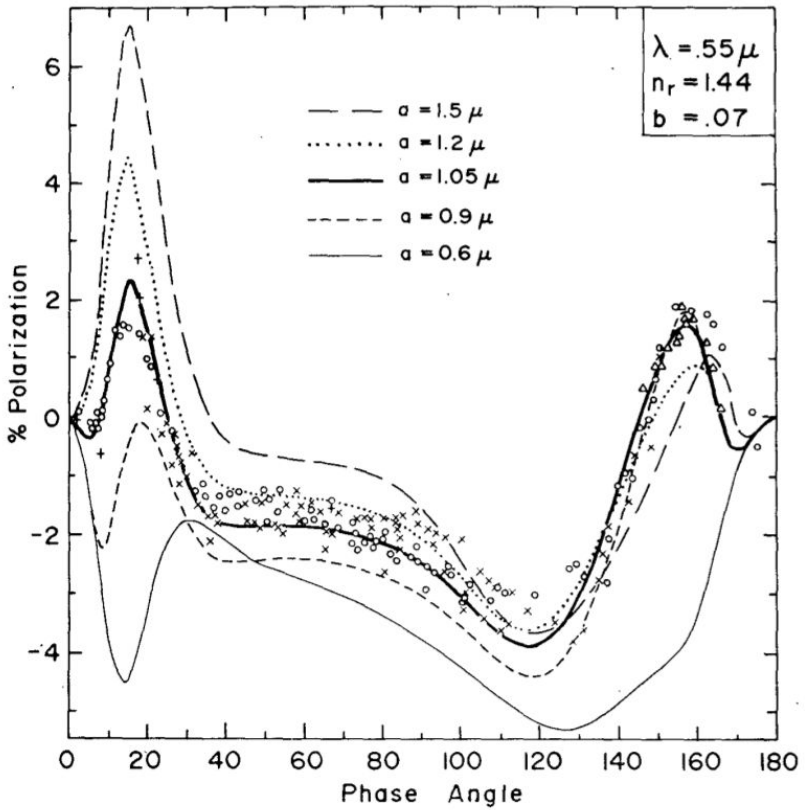

FIG. 4. Observations of the polarization of sunlight reflected by Venus in the visual wavelength region and theoretical computations for $\lambda = 0.55$ μm. The ○'s are wide-band visual observations by Lyot (1929) while the other observations are for an intermediate bandwidth filter centered at $\lambda = 0.55$ μm; the ×'s were obtained by Coffeen and Gehrels (1969), the +'s by Coffeen (cf. Dollfus and Coffeen, 1970), and the Δ's (which refer to the central part of the crescent) by Veverka (1971). The theoretical curves are all for a refractive index 1.44, the size distribution (8) with $b = 0.07$, and a Rayleigh contribution $f_R = 0.045$. The different curves show the influence of the effective radius on the polarization.

(Effect of changes in variance)

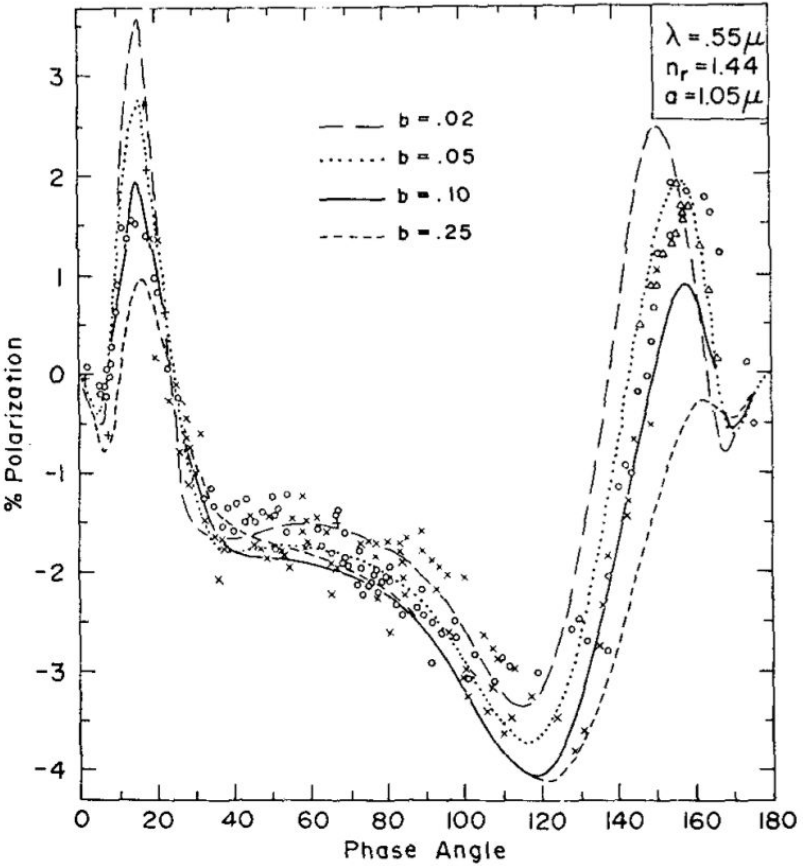

FIG. 5. As in Fig. 4 except that all of the theoretical curves are for $a = 1.05$ μm, while the effective variance is allowed to range over the values 0.02 to 0.25.

(Effect of changes in refractive index)

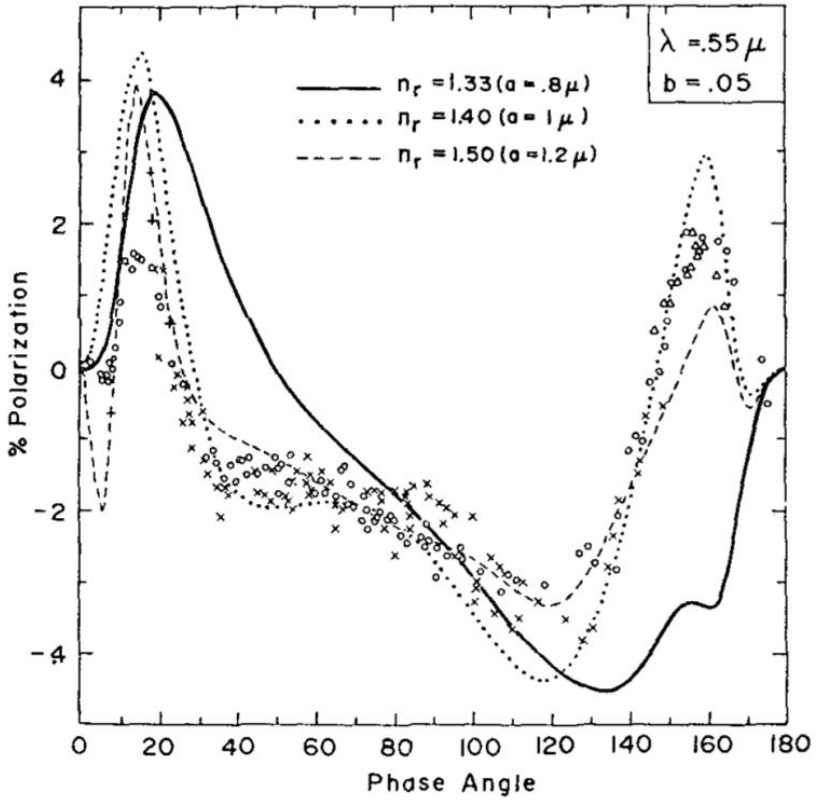

FIG. 6. Observations are the same as in Fig. 4. The theoretical curves are for three refractive indices with the effective particle radius chosen in each case to yield the best agreement with the observations. The size distribution is (8) with $b=0.05$. The Rayleigh contribution to the phase matrix is given by $f_R=0.045$

(Effect of changes in Rayleigh component)

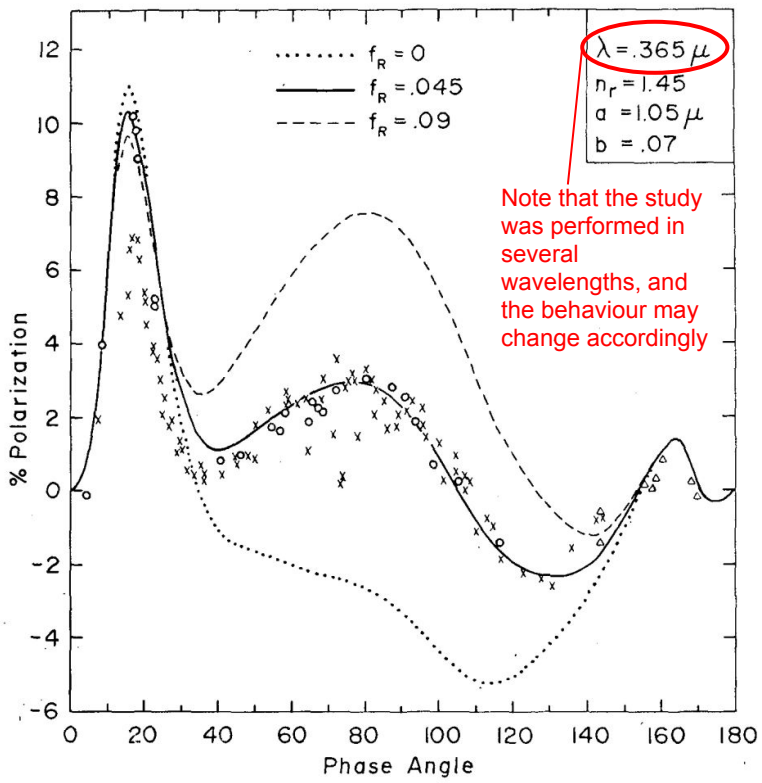

Note that the study was performed in several wavelengths, and the behaviour may change accordingly

FIG. 9. Observations and theoretical calculations of the polarization of sunlight reflected by Venus at $\lambda=0.365$ μm. The observations were made with intermediate bandwidth filters centered at $\lambda=0.365$ μm, the ×'s being obtained by Coffeen and Gehrels (1969) in 1959–67, the ○'s by Coffeen in 1967–69 (cf. Dollfus and Coffeen, 1970), and the △'s by Dollfus in 1969 (cf. Dollfus and Coffeen, 1970). The observations of Coffeen and Gehrels refer to the entire visible planetary disk, while those of Dollfus refer to an area on the disk midway between limb and terminator. The theoretical curves are the results after integration over the visible disk. They are for a homogeneous atmosphere containing spherical particles of the size distribution (8) with $a=1.05$ μm and $b=0.07$. The refractive index of the particles is 1.45. The three theoretical curves are for different Rayleigh contributions to the phase matrix.

1974 - Venus atmosphere

Comparison between model and laboratory measurements

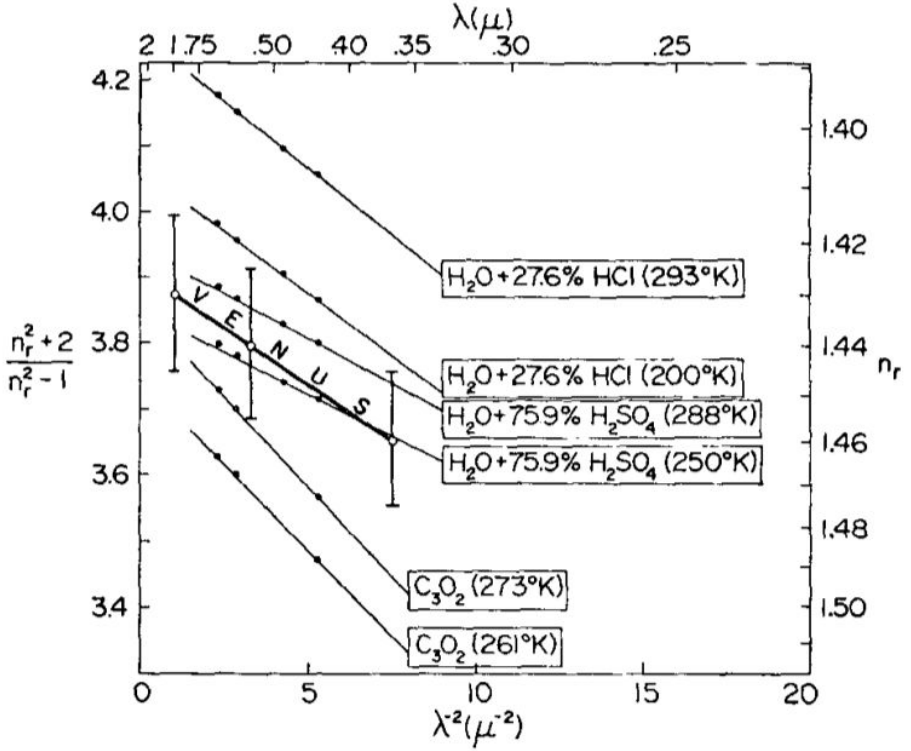

FIG. 14. Refractive indices of the Venus cloud particles (open circles) deduced from the polarization. The error bars represent the maximum uncertainty, not a probable error. The experimental values (dots) for the indicated liquids are based on laboratory measurements and, in some cases, interpolation formulas, as explained in the text.

1974 - Venus atmosphere

The conclusions of Hansen and Hovenier's work were:

- n_r=1.44 ± 0.015 at λ = 550nm (although described in several wavelengths).
- Spherical shapes with r_{eff}=1.05 ± 0.10 μm and v_{eff}=0.07 ± 0.02.
- Pressure at the cloud tops: ~50 ± 25mb.
- Composition: concentrated sulfuric acid.

The Titan’s mystery

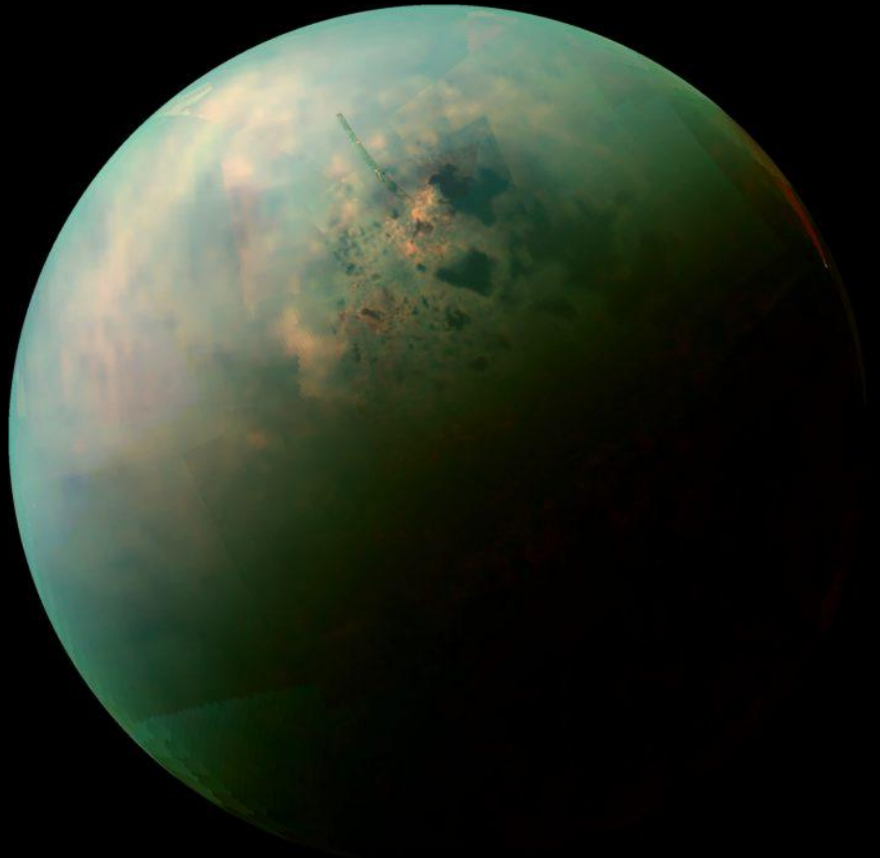

NASA | JPL-Caltech | University of Arizona | University of Idaho

The Titan's mystery

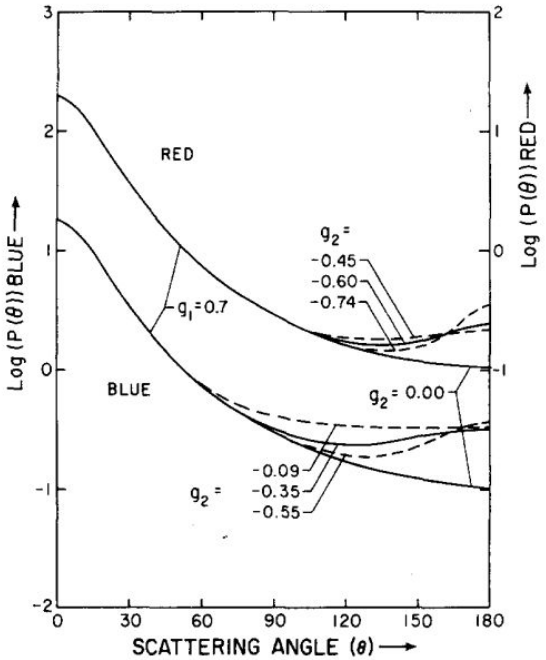

Intensity observed at high phase angle (small scattering angle) requires mean radius in the range 0.14-0.25 μm.

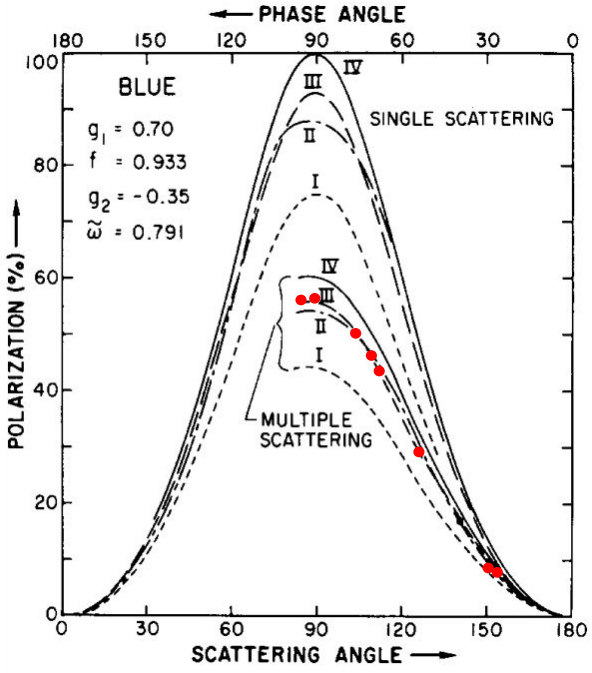

Strong linear polarization requires mean radii no larger than 0.1 μm.

(Tomasko and Smith, 1982)

The Titan's mystery

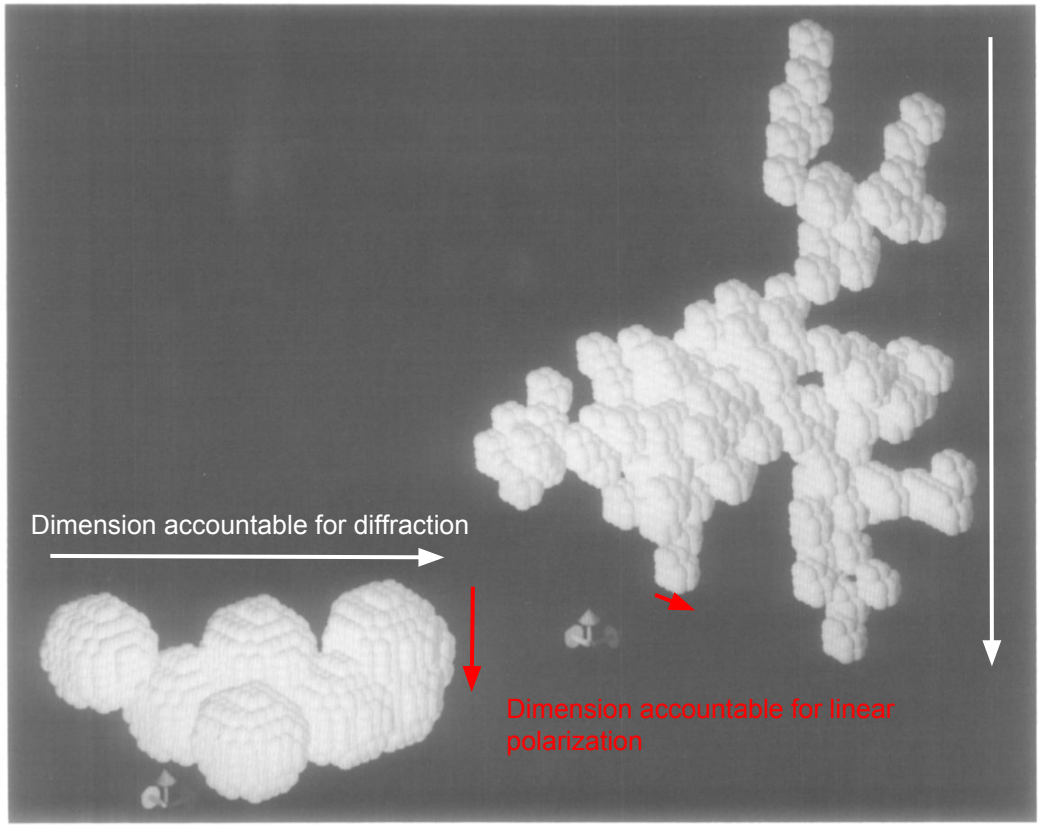

FIG. 1. This synthetic image shows the type I (right) and II aggregate particles discussed in the text. Individual dipole elements (for the discrete dipole array calculation) are shown as small spheres. Arrows indicate unit vector directions in the lattice coordinate system used to construct the particles.

(West, 1991)

Spectropolarimetric biosignatures in Earth-like exoplanets

Spectropolarimetric biosignatures in Earth-like exoplanets

What kind of information could we get from spectropolarimetric observations:

- Clouds and aerosols.
- By surface reflection: % ocean, % vegetation.
- Atmospheric composition.
- Mean cloud height.

Spectropolarimetric biosignatures in Earth-like exoplanets

LETTER

doi:10.1038/nature10778

Biosignatures as revealed by spectropolarimetry of Earthshine

Michael F. Sterzik[1], Stefano Bagnulo[2] & Enric Palle[3]

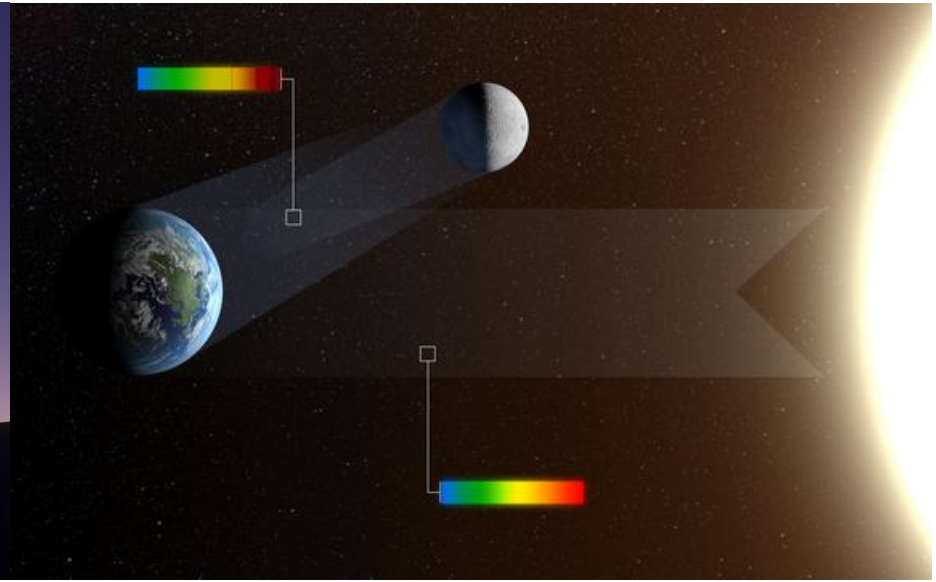

Spectropolarimetric biosignatures in Earth-like exoplanets

The lunar depolarization factor is not well determined, but roughly correlates with the albedo of the reflecting surfaces[19,20]. Following a classic study[14], we assume a linear increase of depolarization (depol) with wavelength, normalized to 3.3 at a wavelength at 550 nm (depol = $3.3\lambda/550$, where λ is in units of nm).

Spectropolarimetric biosignatures in Earth-like exoplanets

The lunar depolarization factor is not well determined, but roughly correlates with the albedo of the reflecting surfaces[19,20]. Following a classic study[14], we assume a linear increase of depolarization (depol) with wavelength, normalized to 3.3 at a wavelength at 550 nm (depol = $3.3\lambda/550$, where λ is in units of nm).

1957

Methodology I: Performance test

Asymmetry parameter

$$g = \int_0^{\pi} \mathrm{d}\theta \sin\theta \cos\theta F_{11}^{\mathrm{syn}}(\theta)$$

Phase function

Degree of linear polarization for unpolarized incident light

Backscattering depolarization factor

$$\delta_L = \frac{F_{11}(\pi) - F_{22}(\pi)}{F_{11}(\pi) + F_{22}(\pi)}$$

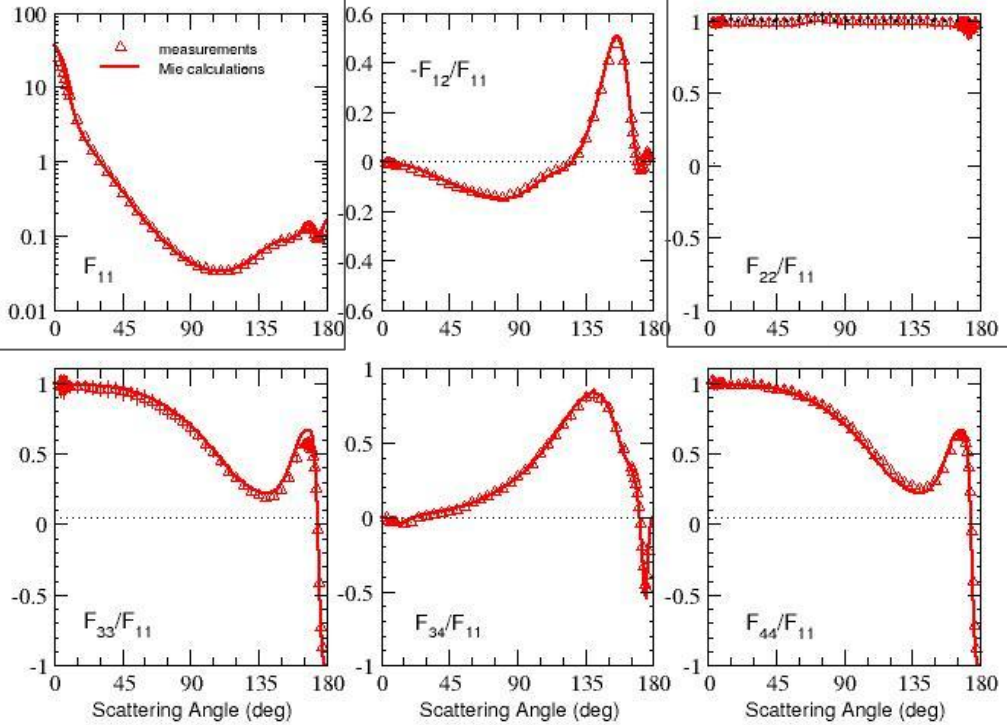

Water droplets scattering matrix

Space weathering

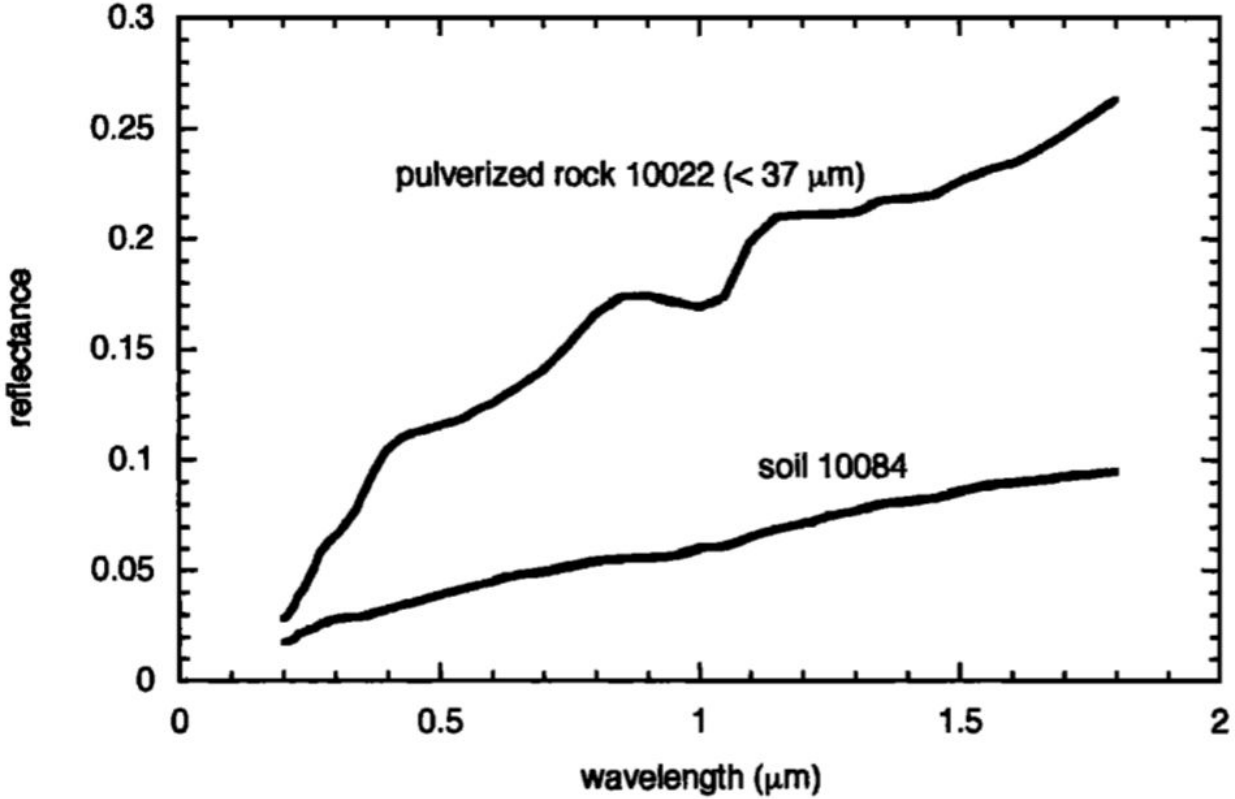

Hapke, 2001.

Figure 2. Bidirectional reflectance spectra ($i = e = 30°$, $g = 60°$, where i is the incidence angle, e is the viewing angle and g is the phase angle), relative to a MgO standard, of Apollo 11 lunar soil sample 10084 and lunar rock 10022 pulverized to < 37 μm.

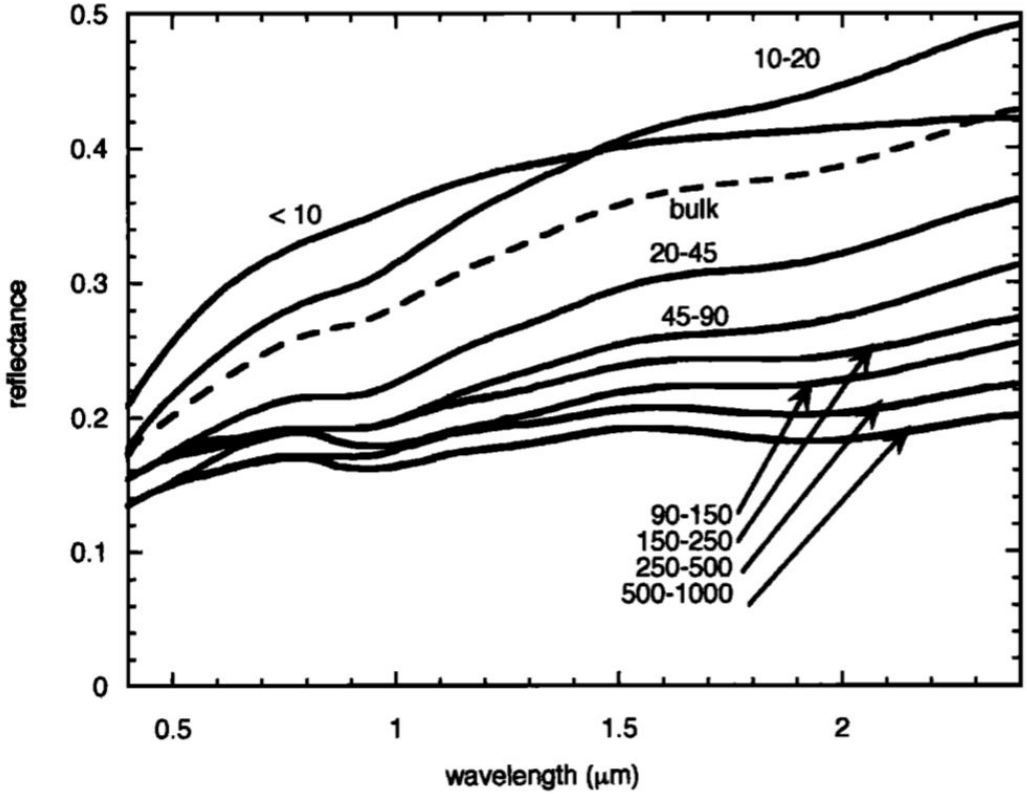

Hapke, 2001.

Figure 3. Bidirectional reflectance spectra ($i = 30^o$, $e = 0$, $g = 30^o$, relative to a polytetrafluoroethylene (PFE) standard) of seprated size fractions (in μm) of lunar soil sample 67701 [*Fischer and Pieters*, 1994]. The fractions were wet - sieved in liquid freon. Subsequent investigation [*Noble et al.*, 2001] showed that soaking a silicate powder in freon affected its spectrum in such a way as to change the amplitude, but not the general shape of the reflectance curve. (Data generously furnished by C. Pieters.)

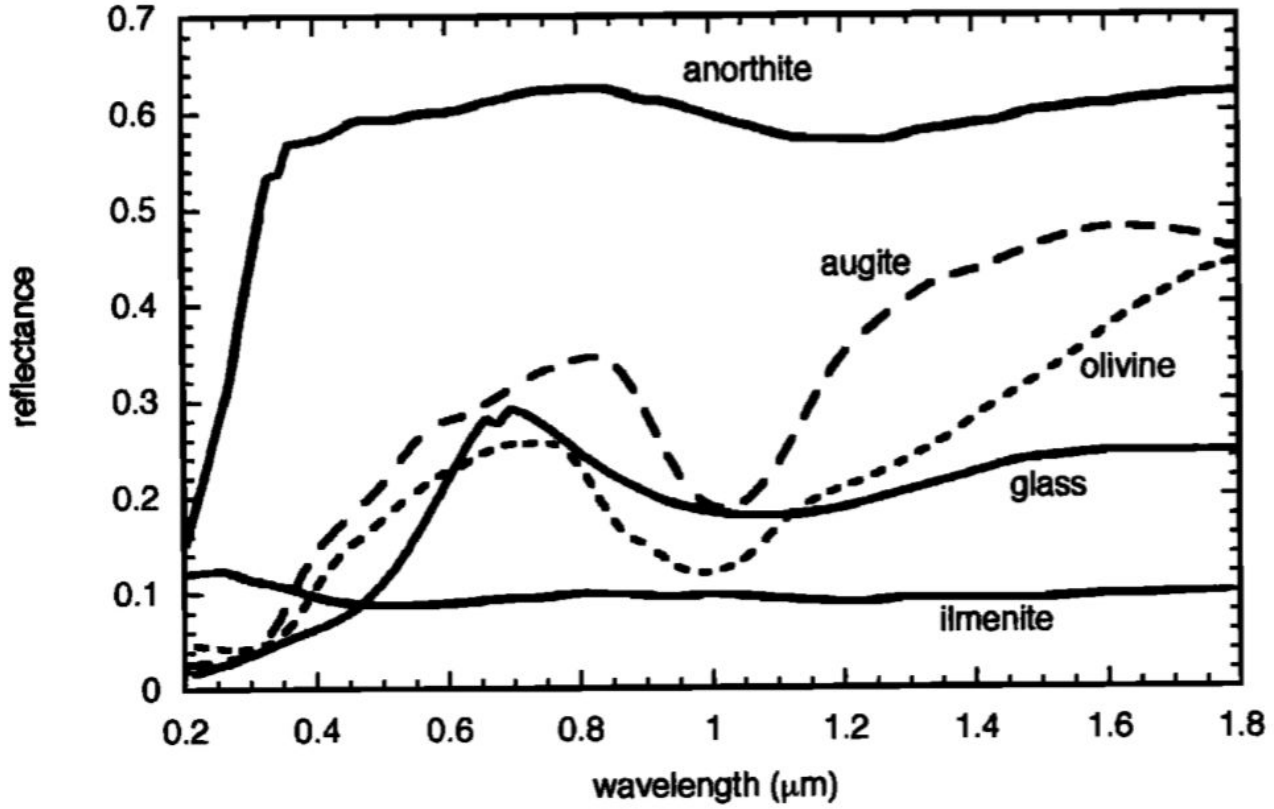

Hapke, 2001.

Figure 4. Bidirectional reflectance spectra ($i = e = 30^o$, $g = 60^o$, relative to a $BaSO_4$ standard) of the major minerals found on the lunar surface, pulverized to < 74 μm (data from *Wagner et al.* [1987]).

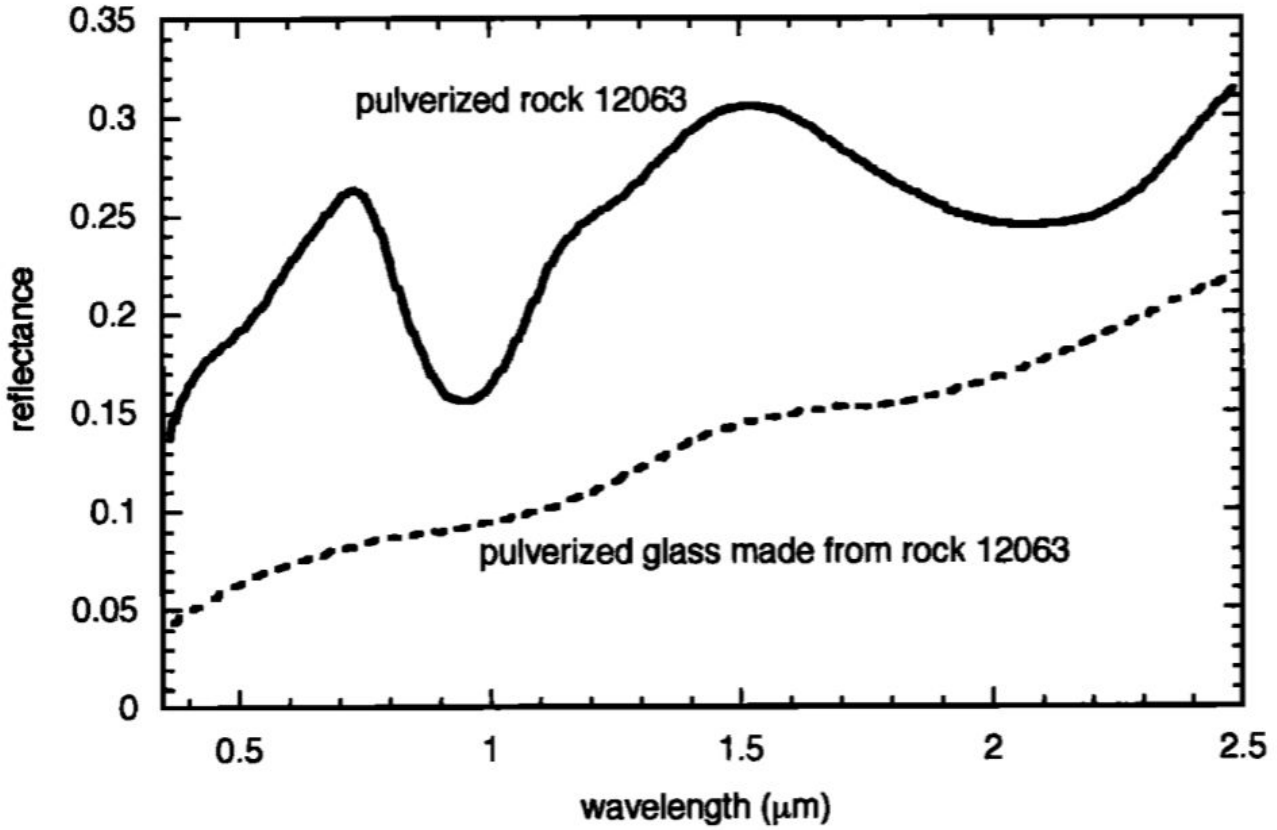

Hapke, 2001.

Figure 5. Hemispherical reflectance spectra (relative to an MgO standard) of lunar rock 12063 and glass made by melting the same rock in N_2, both pulverized to 125-500 μm (data from *Adams and McCord* [1971]).

Results from Hapke et al. 1975.

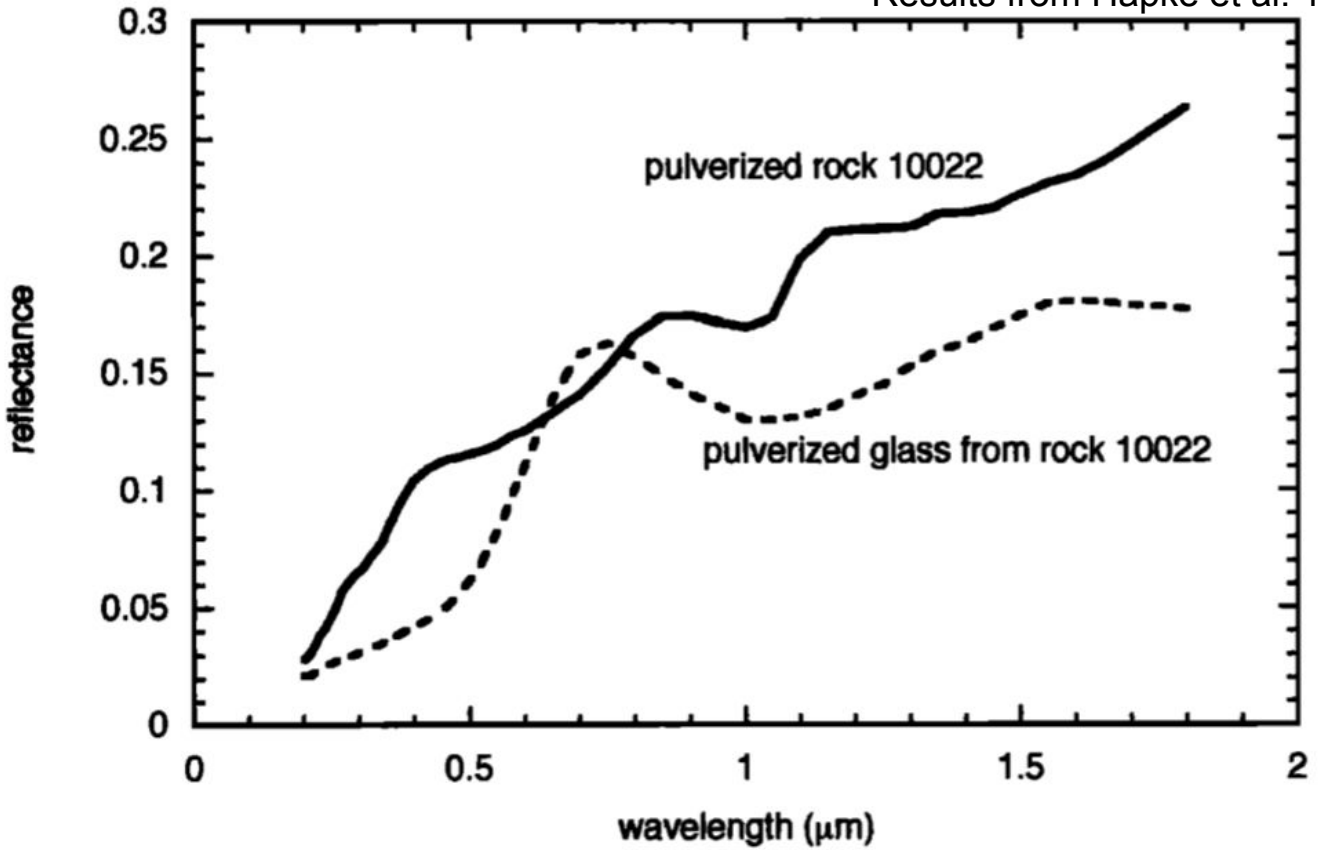

Hapke, 2001.

Figure 6. Bidirectional reflectance spectra ($i = e = 30^o$, $g = 60^o$, relative to a $BaSO_4$ standard) of lunar rock 10022 and glass made by melting the same rock in vacuo, both pulverized to < 37 μm.

After a detailed investigation *Wells and Hapke* [1977] showed that the reason for the discrepancies very probably was the differing environments in which the vitrifications were carried out, which caused the Fe in the samples to have different valence states. *Conel and Nash* [1970] and *Adams and McCord* [1971] had melted their samples in a Pt crucible in flowing commercial N_2 gas at 1 atm pressure, whereas *Hapke et al.* [1975a] had melted their lunar rocks in a high vacuum, reasoning that this was the best terrestrial analog to lunar vitrification conditions. Commercial N_2 typically contains of the order of 0.1% impurities, chiefly O_2 and H_2O. Such an environment is well above the FeO-Fe_2O_3 phase boundary and, hence, is highly oxidizing. In addition, a Pt crucible can act as a catalyst in the reaction $Fe^{2+} \longrightarrow Fe^0 + Fe^{3+}$, with the Fe^0 alloying with the Pt [*Cassidy and Hapke*, 1975]. Ferric iron has strong allowed absorption bands in the visible part of the spectrum.

Hapke, 2001.

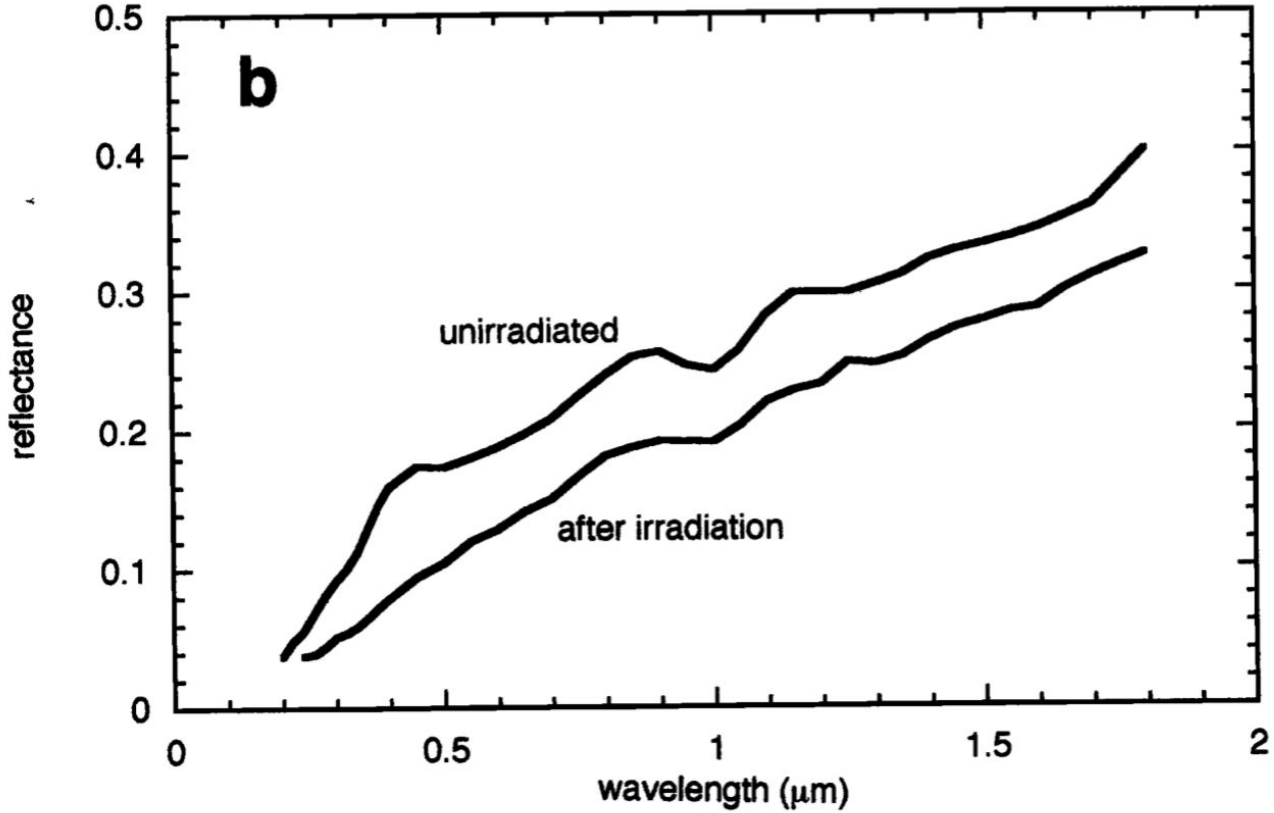

Hapke, 2001.

Figure 7. Effects of a simulated solar wind of 2 keV H ions on silicate powders. (a) From left to right: unirradiated pulverized lunar rock 10022; irradiated powdered rock; and lunar soil 10084. (b) Spectra of the unirradiated and irradiated 10022 powdered rock shown in Figure 7a. (c) Powdered terrestrial rocks and minerals before (top images) and after (bottom images) H - ion irradiation. Figure 7c is reproduced from *Hapke* [1966] with the kind permission of the Johns Hopkins University Press.

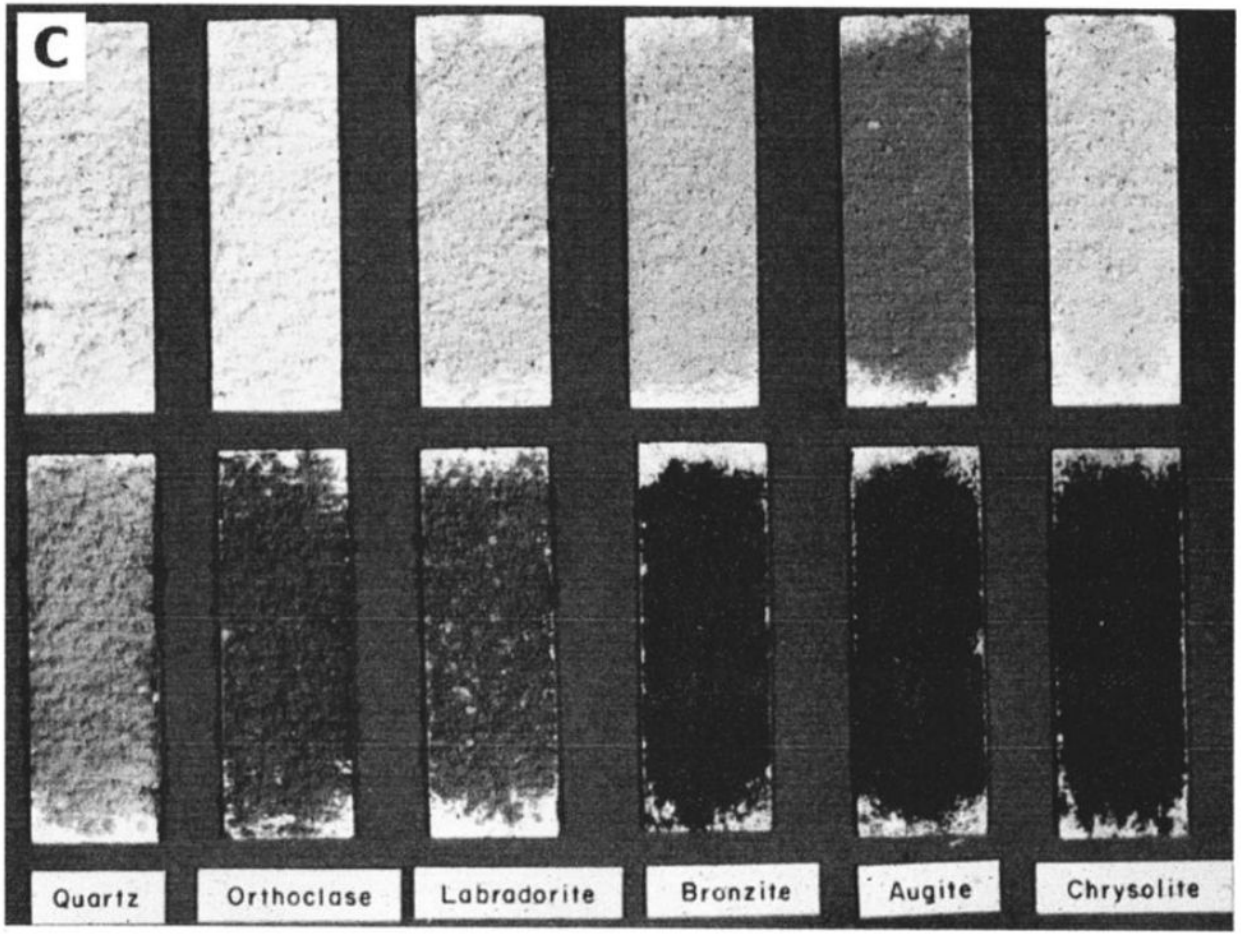

Figure 7. (continued)

Hapke, 2001.

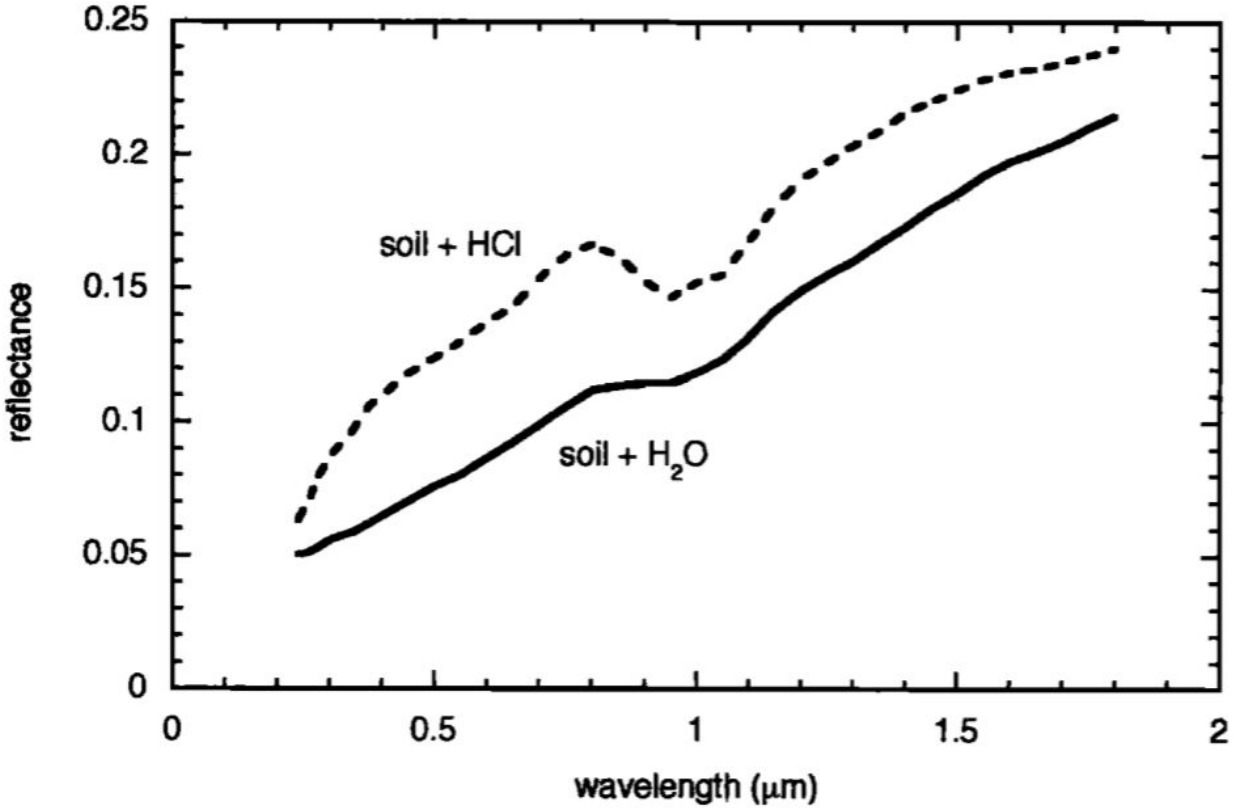

Hapke, 2001.

Figure 15. Bidirectional reflectance spectra ($i = e = 30^o$, $g = 60^o$, relative to a MgO standard) of lunar soil 10084 after soaking in distilled water and in a solution of 20% HCl for 2 hours. The leaching changed the spectrum so that it more closely resembled that of an Apollo 11 rock.

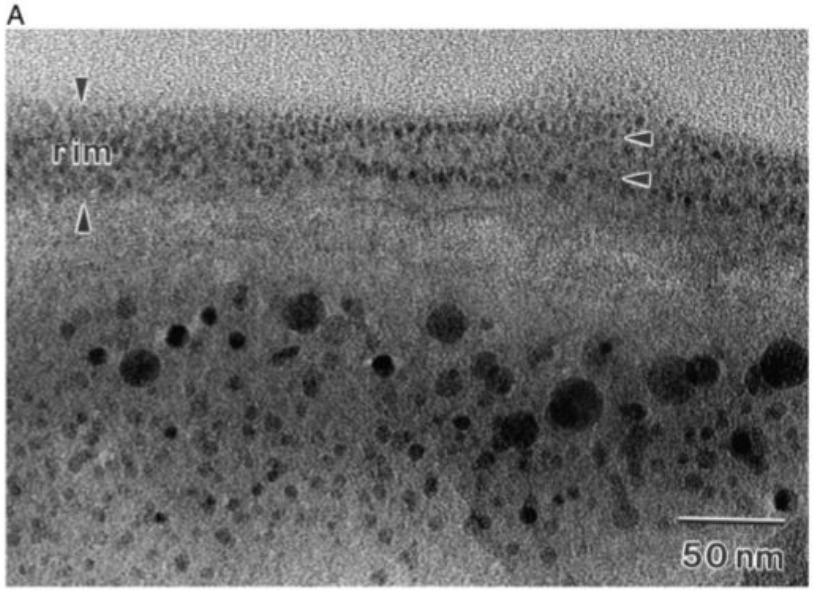

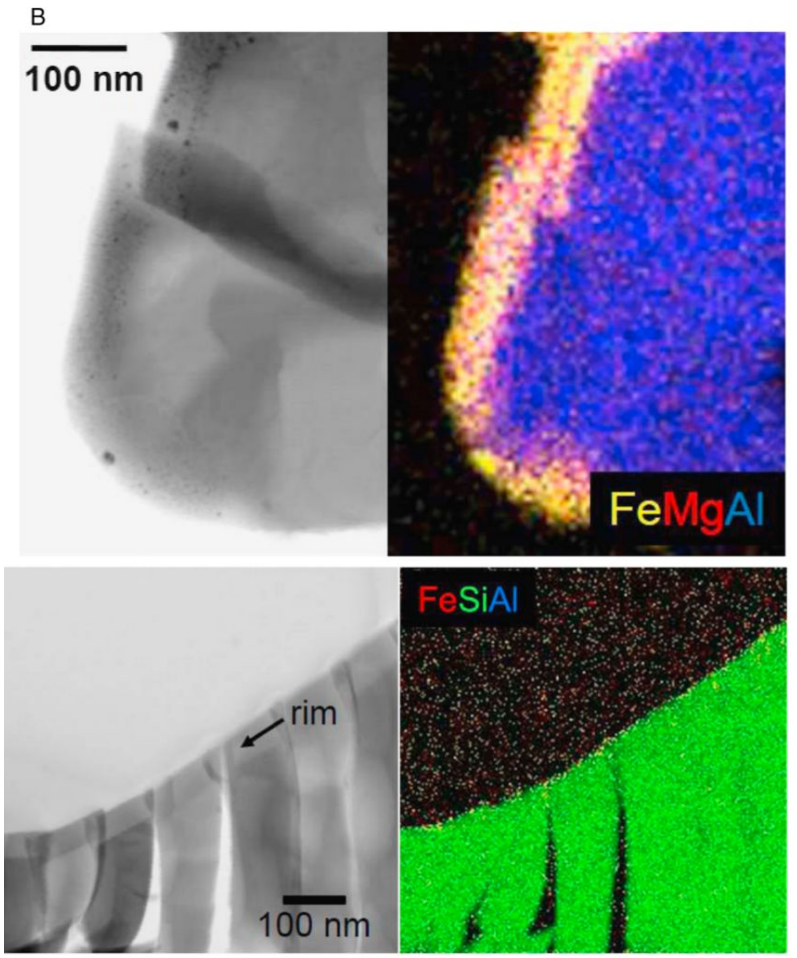

Pieters and Noble, 2016.

Space weathering

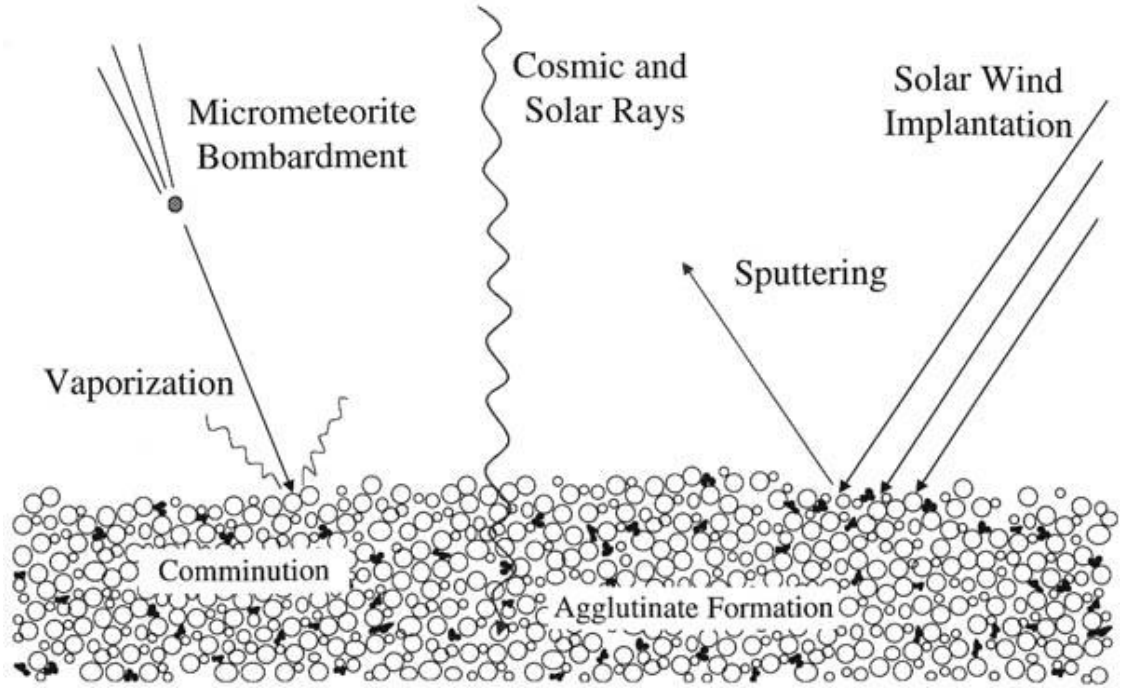

Phenomena that trigger the space weathering (S. Noble)

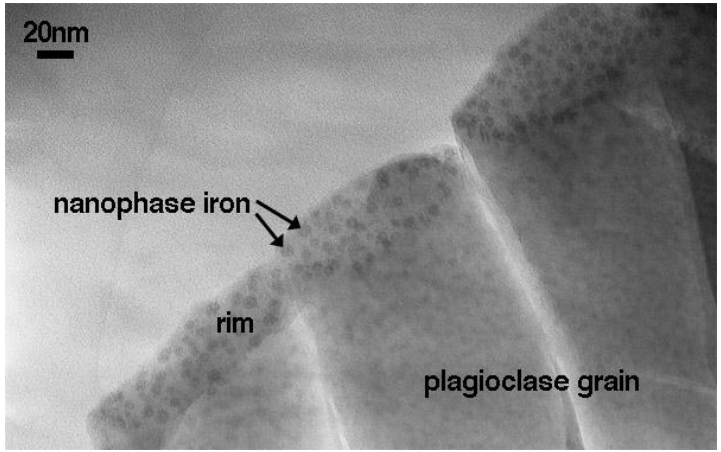

Nanophase iron in rims (S. Noble)

Simulations: particle model

Particle model

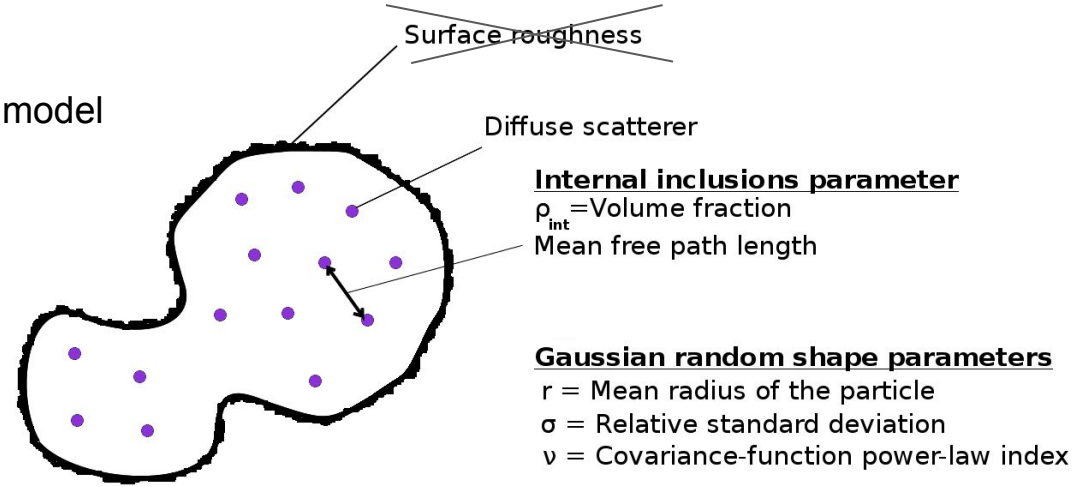

Simulations: particle model

Non-weathered model parameters:

- r=33.5 μm
- σ=0.2
- v=3.3
- l_{min} =2
- l_{max} =11
- m_{host}=1.67+i k_{host}

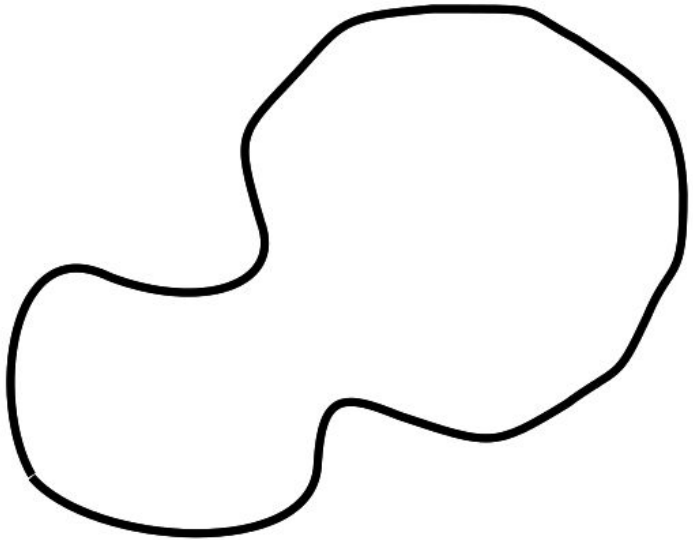

Variable to compute the model

Space weathering effects over reflectance spectrum

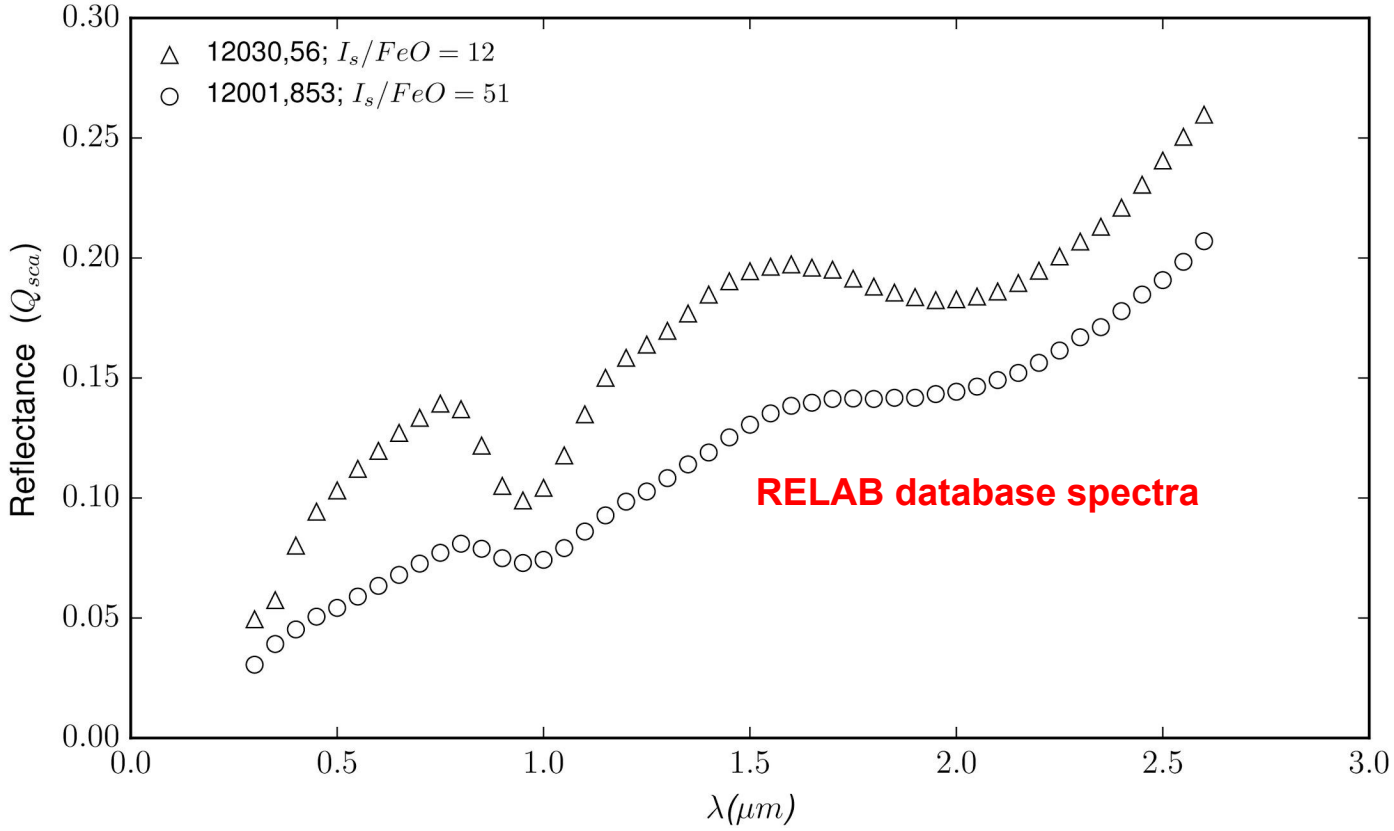

Escobar-Cerezo et al. (ApJ, 2018)

Space weathering effects over reflectance spectrum

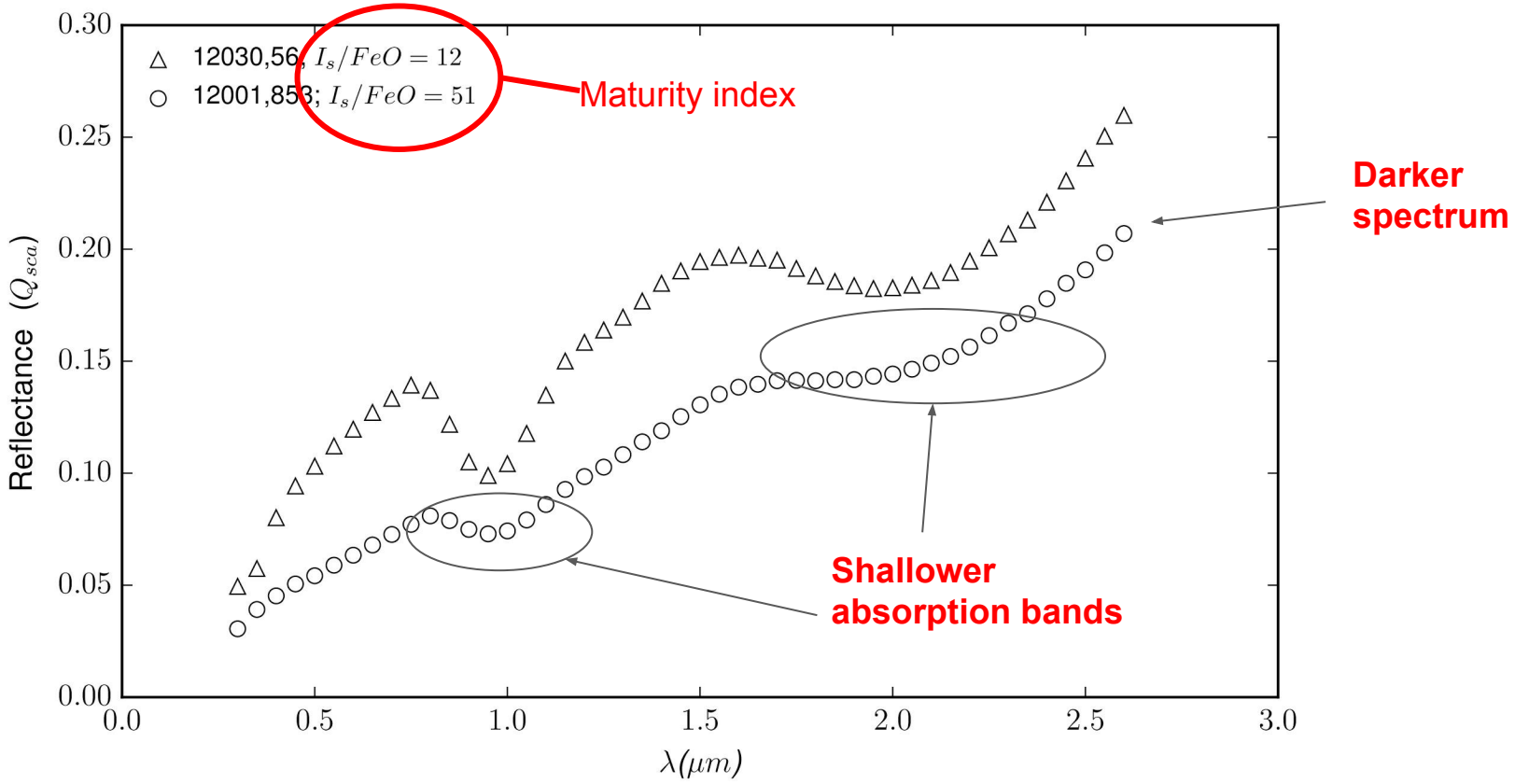

Escobar-Cerezo et al. (ApJ, 2018)

Space weathering effects over reflectance spectrum

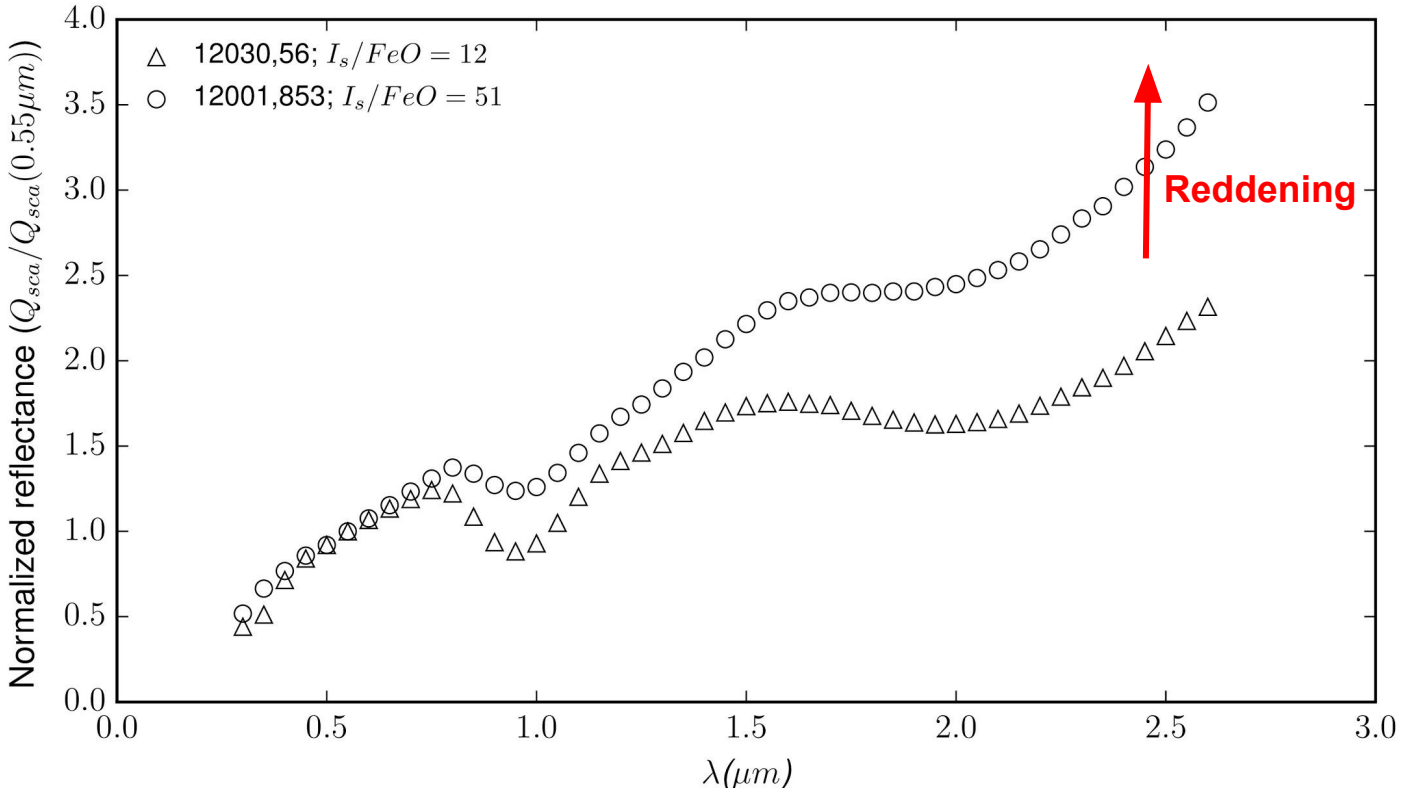

Escobar-Cerezo et al. (ApJ, 2018)

Simulations: modeling the imaginary part of the refractive index

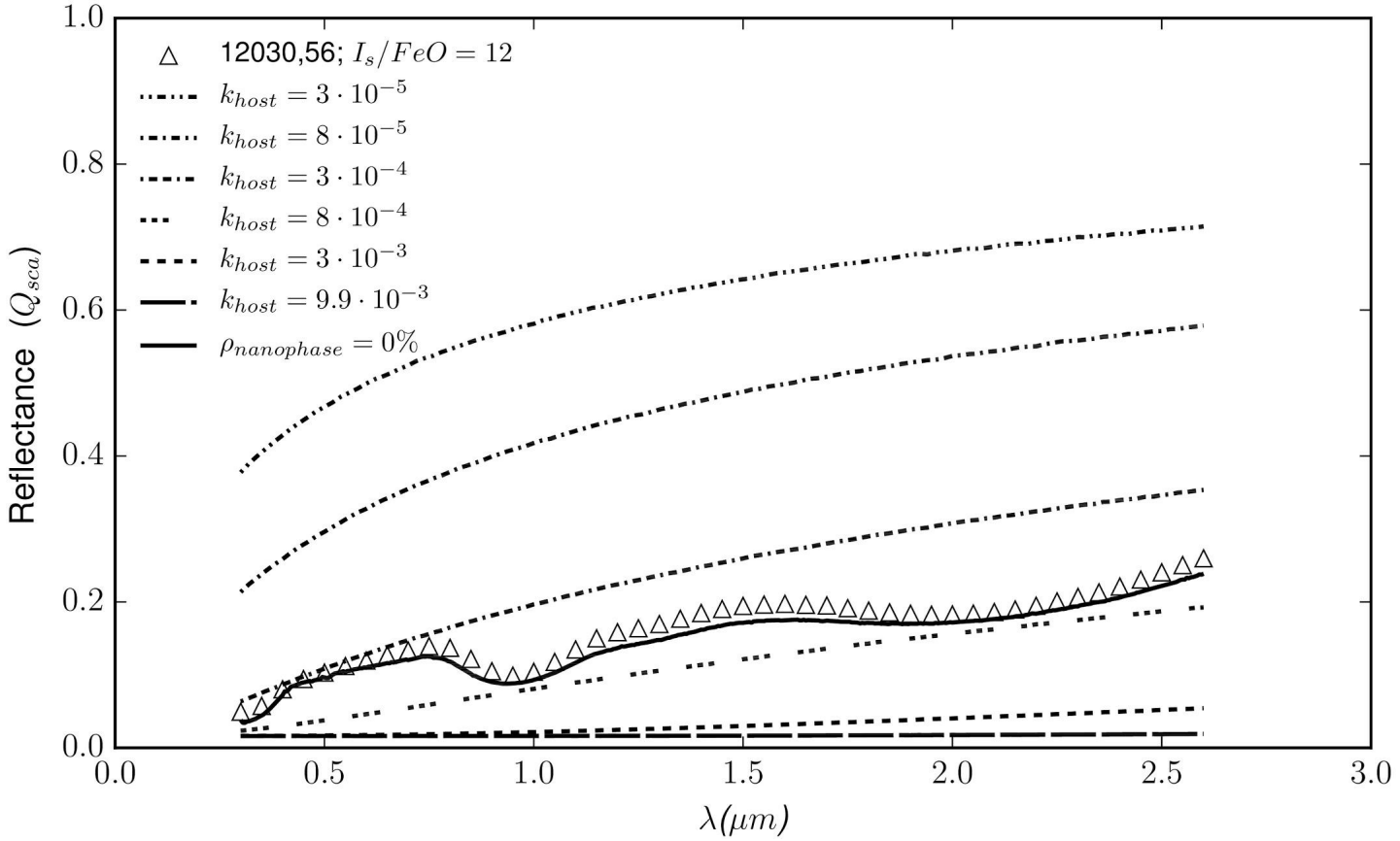

Escobar-Cerezo et al. (ApJ, 2018)

Simulations: modeling the imaginary part of the refractive index

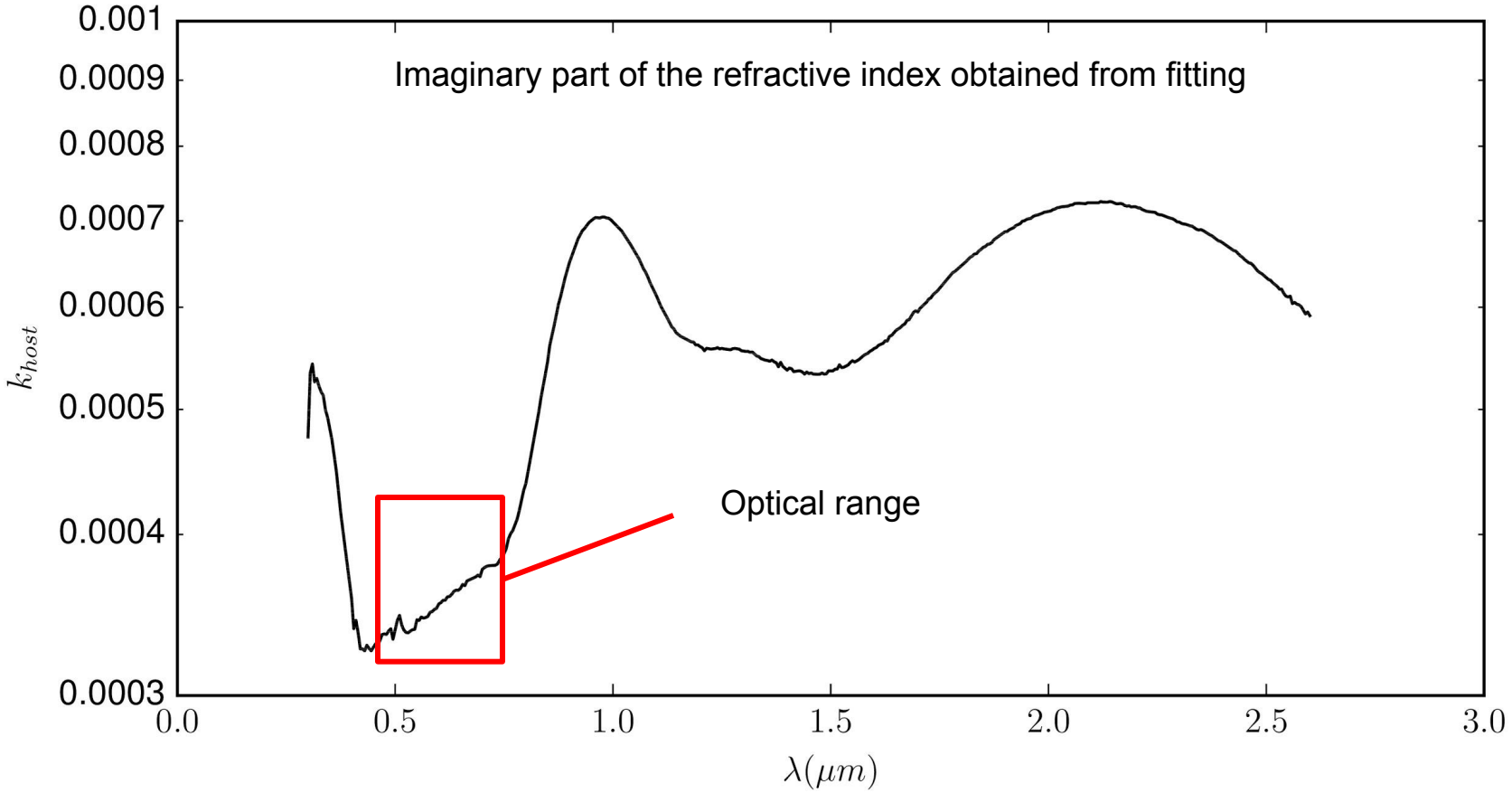

Escobar-Cerezo et al. (ApJ, 2018)

Simulations: spectra models

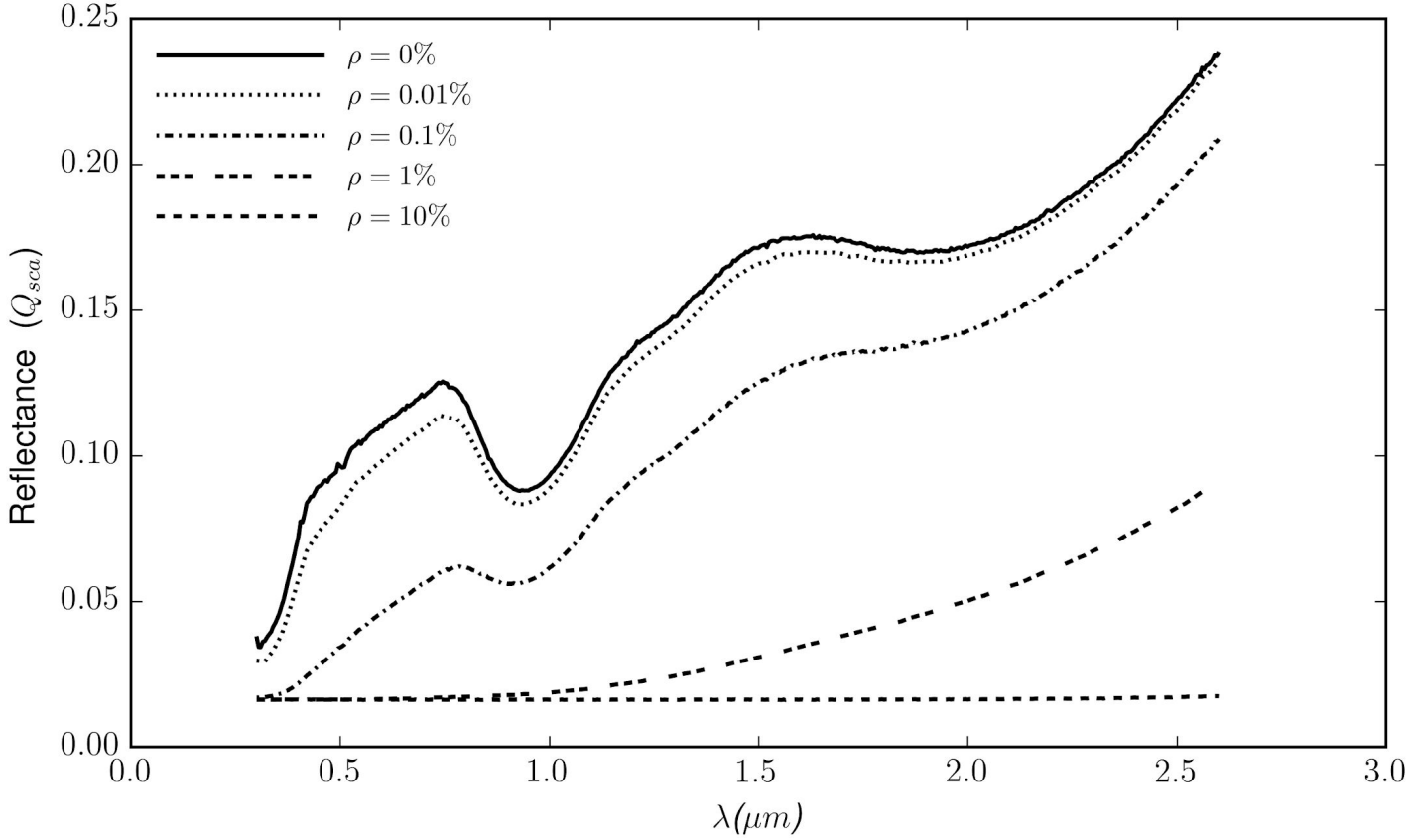

Escobar-Cerezo et al. (ApJ, 2018)

Simulations: spectra models

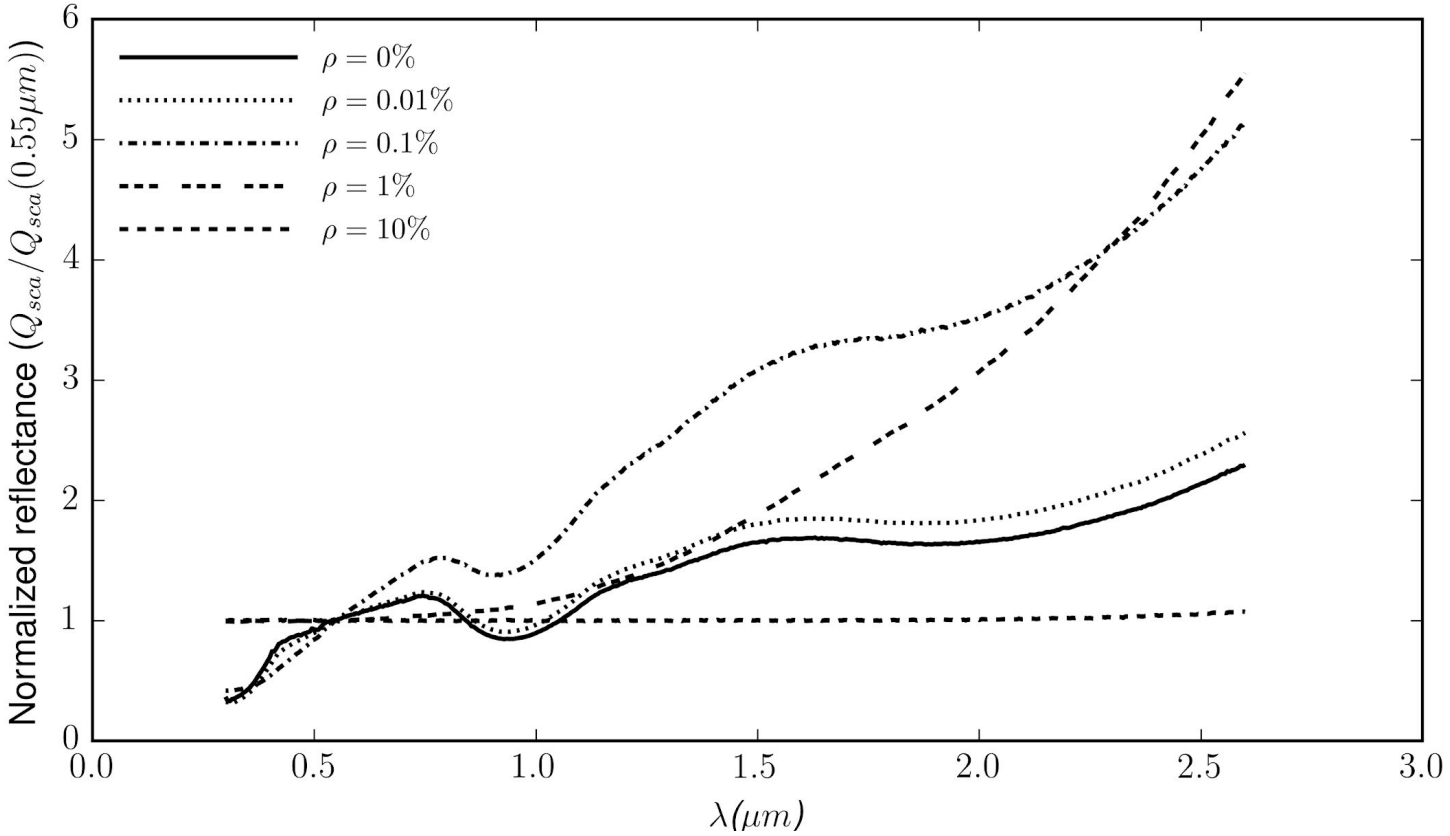

Escobar-Cerezo et al. (ApJ, 2018)

Simulations: comparison between spectra models and experimental spectrum

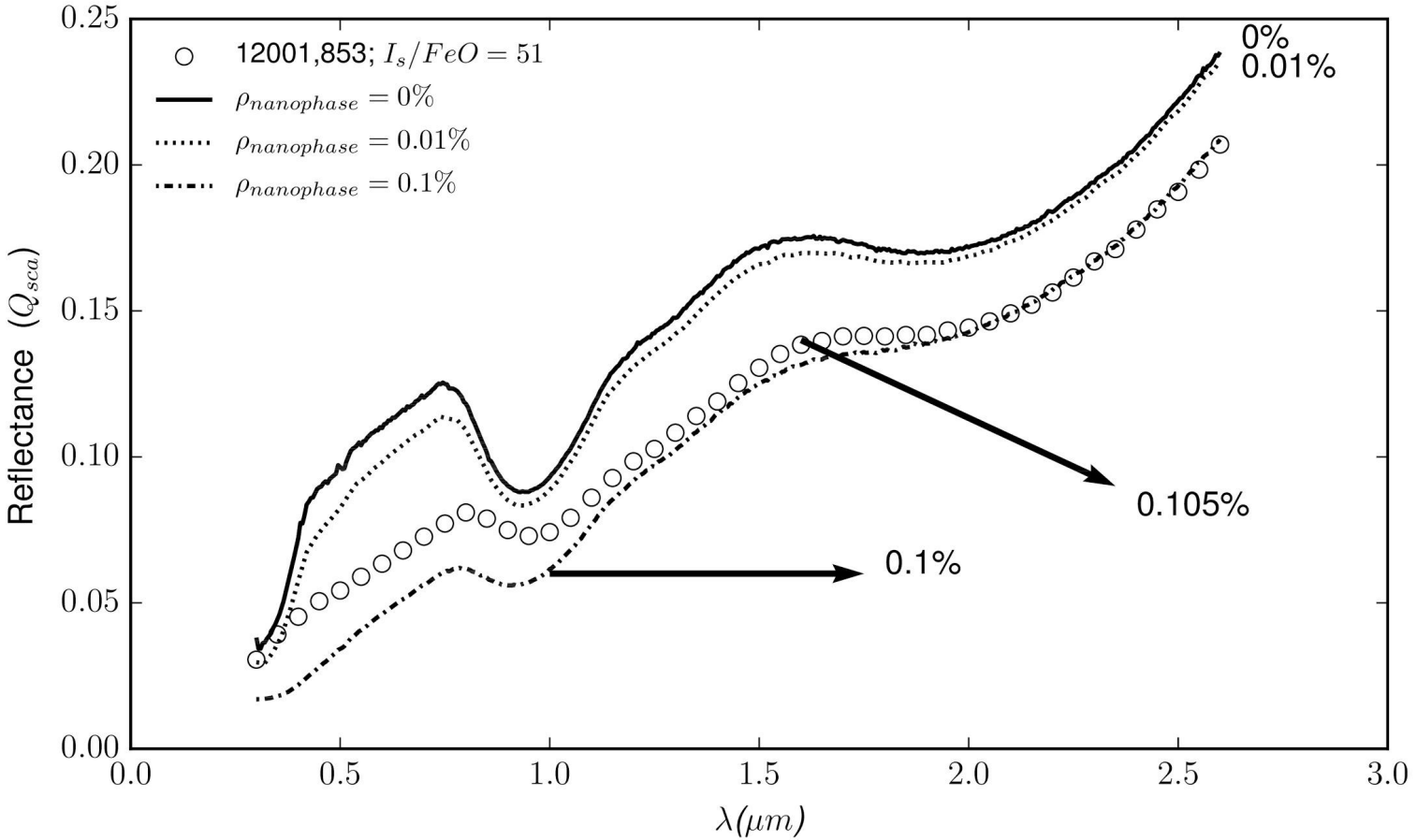

Escobar-Cerezo et al. (ApJ, 2018)

Simulations: comparison between spectra models and experimental spectrum

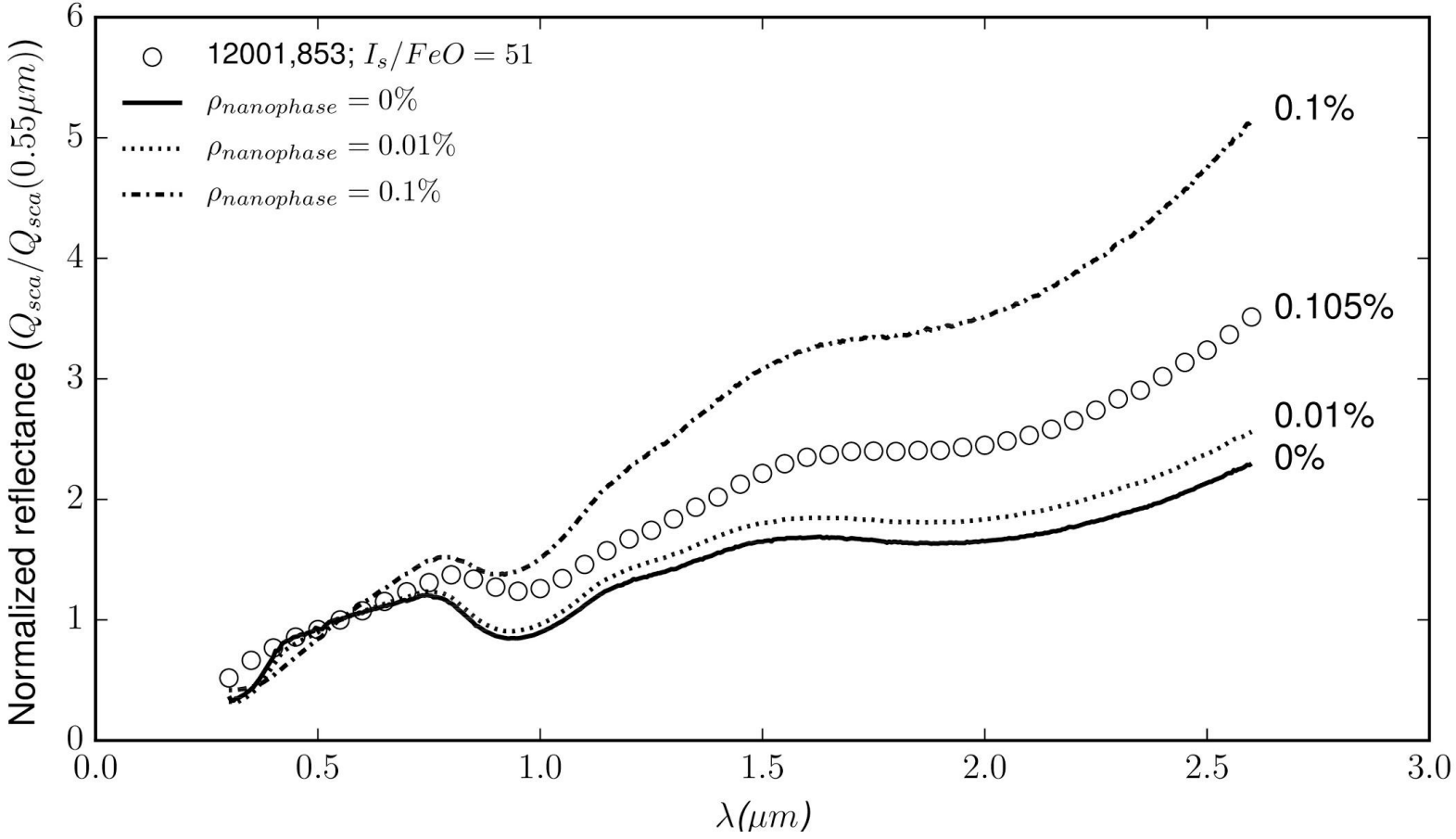

Escobar-Cerezo et al. (ApJ, 2018)

Some references

- Review article about history of space weathering - Bruce Hapke, 2001.
- Review article about space weathering - Pieters and Noble, 2016.
- Britt and Pieters, 1994. For “large” space weathering products.